The Astrophysical Journal, 851:1 (18pp), 2017 December 10 https://doi.org/10.3847/1538-4357/aa9897

On the Dependence of the X-Ray Burst Rate on Accretion and Spin Rate

Yuri Cavecchi[1,2], Anna L. Watts[3], and Duncan K. Galloway[4,5]
[1] Department of Astrophysical Sciences, Princeton University, Peyton Hall, Princeton, NJ 08544, USA; cavecchi@astro.princeton.edu
[2] Mathematical Sciences and STAG Research Centre, University of Southampton, SO17 1BJ, UK
[3] Anton Pannekoek Institute for Astronomy, University of Amsterdam, Postbus 94249, 1090 GE Amsterdam, The Netherlands
[4] School of Physics and Astronomy, Monash University, Clayton, VIC 3800, Australia
[5] Monash Centre for Astrophysics, Monash University, VIC 3800, Australia
Received 2017 October 12; revised 2017 November 2; accepted 2017 November 3; published 2017 December 5

Abstract

Nuclear burning and its dependence on the mass accretion rate are fundamental ingredients for describing the complicated observational phenomenology of neutron stars (NSs) in binary systems. Motivated by high-quality burst rate data emerging from large statistical studies, we report general calculations relating the bursting rate to the mass accretion rate and NS rotation frequency. In this first work, we ignore general relativistic effects and accretion topology, although we discuss where their inclusion should play a role. The relations we derive are suitable for different burning regimes and provide a direct link between parameters predicted by theory and what is to be expected in observations. We illustrate this for analytical relations of different unstable burning regimes that operate on the surface of an accreting NS. We also use the observed behavior of the burst rate to suggest new constraints on burning parameters. We are able to provide an explanation for the long-standing problem of the observed decrease of the burst rate with increasing mass accretion that follows naturally from these calculations: when the accretion rate crosses a certain threshold, ignition moves away from its initially preferred site, and this can cause a net reduction of the burst rate due to the effects of local conditions that set local differences in both the burst rate and stabilization criteria. We show under which conditions this can happen even if locally the burst rate keeps increasing with accretion.

Key words: methods: analytical – nuclear reactions, nucleosynthesis, abundances – stars: neutron – X-rays: bursts

1. Introduction

When a compact object with a solid surface such as a neutron star (NS) is part of a binary system with a less evolved companion, accretion onto the compact object may start, which will lead to the burning of the fresh fuel accumulated on the surface of the NS. If the heating due to the burning is not compensated by cooling, the burning will become unstable, resulting in bright X-ray flashes: the so-called type I bursts (see Strohmayer & Bildsten 2006). A complete description of the phenomenology of the observed bursts depends on various factors, such as accretion physics (Inogamov & Sunyaev 1999, 2010), thermonuclear reaction network physics (Fujimoto et al. 1981; Cumming & Bildsten 2000; Cumming 2003; Woosley et al. 2004; Heger et al. 2007a; Cyburt et al. 2016), and hydrodynamics that may regulate the flame propagation across the surface following localized ignition (Zingale et al. 2001, 2015; Malone et al. 2011; Cavecchi et al. 2013, 2015, 2016).

The implications of a complete understanding of the bursts go well beyond a pure description of thermonuclear flashes. Studying the effects of the outcome of the burning can help in understanding the structure of the compact object. For instance, in the case of NSs, type I bursts are one way to constrain the equation of state of the matter on the inside (Miller 2013; Watts et al. 2016), for example by inferring the mass and radius from the pulse profiles of burst oscillations (fluctuations in the light curves of the bursts due to asymmetric surface patterns that emerge during the bursts; see e.g., Watts 2012). Another example is the cooling light curves of the NSs after the accretion outburst, which depend on how much (and where) heat has been deposited by accretion and burning, and also on the structure of the outer layers of the star (Hanawa & Fujimoto 1984; Brown et al. 1998; Brown & Cumming 2009; Wijnands et al. 2013; Schatz et al. 2014), therefore providing a very useful way of exploring NS (crust) properties such as composition, structure, neutrino emission, and superfluid physics. Unfortunately, our understanding of the different ingredients needed for modeling the observations is still limited. This paper will discuss burning physics.

In the standard theoretical picture that emerges from calculations and numerical simulations, how the burning proceeds depends on the burning regimes (e.g., what fuel is available and what has been spent already, which path the nuclear reactions follow, their temperature dependence, and their heat generation rate; see also Schatz 2011) and the accretion rate. The accreted matter accumulates on the surface of the star and sinks to deeper and deeper densities in the ocean, eventually meeting the conditions where burning starts. At this point, burning stability depends on whether or not the cooling is capable of compensating for the heat release. Even at low accretion rates, the burning rate and the energy release may be above the instability threshold and the bursts begin; then, the frequency of the bursts increases with accretion rate. At the same time, accretion releases heat that eventually stabilizes the burning, preventing any bursting (Fujimoto et al. 1981; Bildsten & Brown 1997; Bildsten 1998; Cumming & Bildsten 2000; Keek et al. 2009; Zamfir et al. 2014). The amount of heat generation from accretion comes from the gravitational energy released at the moment of accretion, the compressional heat due to the extra weight of the

accumulated material, and the heat of further reactions that take place deeper than the burning layer (Cumming & Bildsten 2000). However, many details of the burst physics are still uncertain, mainly the reaction rates (e.g., Schatz et al. 2001; Cooper & Narayan 2006a, 2006b; Heger et al. 2007b; Cyburt et al. 2010; Davids et al. 2011; Keek et al. 2014; Cyburt et al. 2016), or, for example, the role of mixing (e.g., Piro & Bildsten 2007; Keek et al. 2009).

One important factor in burst physics is the rotation of the star. First of all, rotation opposes gravity, thus reducing the local effective gravity, which has a direct effect on the local accretion rate and on how the burning proceeds (for example, determining the most likely ignition colatitude; Cooper & Narayan 2007a; AlGendy & Morsink 2014 and see also the next sections). Second, another source of heat that might have significant importance for the burning processes is the heat released by some effective friction that is present at the boundary and the spreading layers between the accretion disk and the surface of the star (Inogamov & Sunyaev 1999, 2010; Kajava et al. 2014; Philippov et al. 2016). For stars with equal mass and radius, the magnitude of this effect will still depend on the spin frequency of the star and how this compares to the velocity of the disk at the star radius. Furthermore, rotation affects the burning by inducing mixing of newly accreted material and ashes from previous bursts in deeper layers. It also has indirect effects since the mixing changes the temperature profile of the layer (Piro & Bildsten 2007; Keek et al. 2009). Once again, the exact dependence of the bursting frequency on the accretion rate and spin frequency is still not well-understood.

As a consequence of all of the uncertainties, observations often do not behave as models predict. For instance, the burning stabilizes and the bursts disappear too early, in terms of the mass accretion rate, with respect to theoretical expectations (e.g., Cornelisse et al. 2003; Cumming 2004; Heger et al. 2007b; but not always; see, for example, Linares et al. 2012). Also, most theoretical works predict that the burst rate should always increase with accretion rate. One notable exception is the delayed mixed-burst regime found by Narayan & Heyl (2003). However, Cooper & Narayan (2007b) caution against conclusions about the time-dependent behavior drawn from linear stability analysis like the one of Narayan & Heyl (2003), and experimental work does not confirm the pre-requisite for delayed mixed bursts (namely, a weaker CNO breakout reaction rate of $^{15}\mathrm{O}(\alpha,\gamma)^{19}\mathrm{Ne}$; Piro & Bildsten 2007; Fisker et al. 2007; Tan et al. 2007). Cooper & Narayan (2007a) also found a burst rate decreasing with increasing accretion rate, but that was due to the delayed burst regime of Narayan & Heyl (2003), which, as we said, is not confirmed by direct experiments. Lampe et al. (2016), using the 1D multizone code KEPLER (Woosley et al. 2004), find a regime with a decreasing burst rate, but do so only in very limited ranges of high accretion rate. Despite the fact that the general understanding would predict a continuously increasing burst rate, the contrary is often observed: in many sources, the burst rate is seen to decrease by as much as an order of magnitude before the bursts stabilize (e.g., van Paradijs et al. 1988; Cornelisse et al. 2003; see also Strohmayer & Bildsten 2006 and references therein); the reason why is still not clear. Burst samples are now sufficiently comprehensive (e.g., the MINBAR catalog; see Galloway et al. 2010) that we are able for the first time to explore in a systematic way the effect of accretion and rotation rates on the burst rate.

In this paper, we present general, if somewhat simplified, calculations that relate burning and accretion physics parametrizations to observed quantities such as burst rate and mass accretion rate.[6] We initially follow a similar approach to that of Cooper & Narayan (2007a), who discussed the effects of NS spin for specific burning regime transitions. We develop the calculations considering the effects of local gravity (Section 2) and we show how effects of mixing can be included in the same formalism (Section 3). We present a general study that covers all of the mathematical possibilities and show which ones would be compatible with observations. This paper is by necessity leaning toward the abstract side, but we hope it would offer a guide to the theoretical efforts and a bridge between theory and observations.

1.1. A New Explanation for Decreasing Burst Rate

The algebra of this paper will be presented fully in the following sections, but since the mathematical steps may hide the physics and the results behind them, we will discuss here the meaning and implications of the calculations and how they compare with the previous standing of the theory of bursts.

We will show that, by generalizing the approach of Cooper & Narayan (2007a), the burst rate of a single source can be parametrized as (Equation (16))

$$\mathcal{R} = \bar{\mathcal{R}} \dot{m}_{\rm p}^{\alpha}\, \bar{g}^{\beta}. \tag{1}$$

$\bar{\mathcal{R}}$, α, and β are constants that depend on the burning regime. $\dot{m}_{\rm p}$ is the local mass accretion rate at the pole, which turns out to be a useful proxy for the global accretion rate $\dot{M}_{\rm tot}$, as measured near the star, to which it is related by (Equation (12))

$$\dot{m}_{\rm p} = \frac{(\nu/\nu_{\rm k})\sqrt{1-(\nu/\nu_{\rm k})^2}}{\arctan\sqrt{\frac{(\nu/\nu_{\rm k})^2}{1-(\nu/\nu_{\rm k})^2}}}\frac{\dot{M}_{\rm tot}}{4\pi R_{\star}} = N(\nu)\dot{M}_{\rm tot}, \tag{2}$$

where $R_{\star}$ is the radius of the star, ν is the spin, and $\nu_{\rm k}$ is the Keplerian frequency at the star surface, $\nu_{\rm k} = \sqrt{GM/R_{\star}^3}\big/2\pi$, so that

$$\mathcal{R} = \bar{\mathcal{R}} N(\nu)^{\alpha}\, \dot{M}_{\rm tot}^{\alpha}\, \bar{g}^{\beta}. \tag{3}$$

The important elements in Equation (3) are $\dot{M}_{\rm tot}^{\alpha}$ and $\bar{g}^{\beta}$. We have different forms for $\bar{g}$. $\bar{g}$ can be related to the colatitude θ of the ignition by (Equation (9))

$$\bar{g} = 1 - \left(\frac{\nu}{\nu_{\rm k}}\right)^2 \sin^2\theta. \tag{4}$$

This equation expresses the correction to the local effective gravity of the star at a given θ due to the centrifugal force. In particular, it expresses the ratio $g_{\rm eff}(\theta,\nu)\big/g_{\rm eff,\,p}$ of the local gravity to the gravity at the pole. Later, we will also suggest that including the effects of mixing should give formulae of a similar form to Equation (3) (and Equations (5) and (6)) with $\bar{g}$

[6] More precisely, mass accretion rate is not directly observed, but it is inferred from the X-ray luminosity under assumptions about the accretion flow and with some information on distance. However, as far as this paper and its calculations are concerned, we consider it to be in the category of "observables."

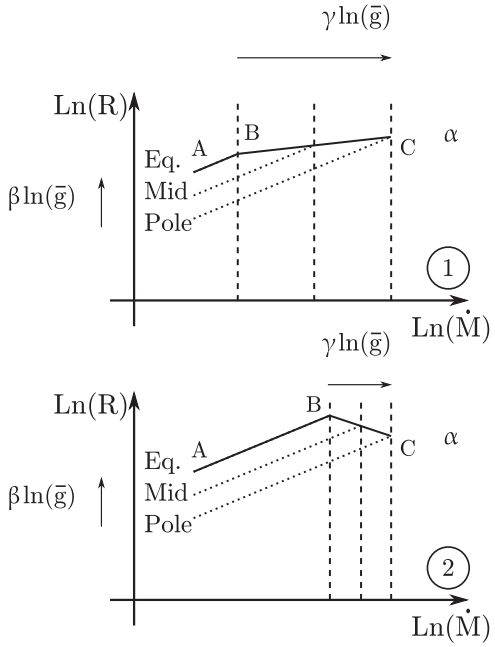

Figure 1. Burst rate $\mathcal{R}$ vs. accretion rate $\dot{M}_{\rm tot}$, solid line. Example for $\alpha > 0$, $\beta < 0$, and $\gamma_{\rm h} > 0$. The inclined dashed lines represent the burst rate at three colatitudes: equator, mid-colatitude, and pole. The slope is α. The equator has the advantage (bursts more often), since $\beta < 0$. How much faster the burst rate of each colatitude is with respect to the pole is given by $\bar{g}^{\beta}$. The three vertical dashed lines indicate the $\dot{M}_{\rm tot}$ at which burning stabilizes at the various colatitudes. Ignition is highest at the equator initially, but then it stabilizes and moves polewards. Depending on the "speed" with which the stabilization moves toward the pole, Case 1 or 2 is realized. The "speed" of stabilization is given by $\Delta \ln \bar{g}/\Delta \ln \dot{M}_{\rm tot} = 1/\gamma_{\rm h}$; $\gamma_{\rm h}$ is the power with which the stabilization $\dot{M}_{\rm tot}$ depends on local conditions. Local conditions depend on the colatitude θ and spin ν. When the vertical lines are "wide," $\gamma_{\rm h}$ is high, such that $\alpha + \beta/\gamma_{\rm h} > 0$: the "speed" is slow and the burst rate keeps growing, Case 1. When the vertical lines are "narrow," $\gamma_{\rm h}$ is small such that $\alpha + \beta/\gamma_{\rm h} < 0$: the "speed" is high and the burst rate is seen to decrease, Case 2.

substituted by another function of ν and θ that is also 1 at the pole and <1 at the equator (see Section 3.1). The effects of mixing should be stronger than those due to changes in effective gravity, making mixing a more plausible cause for the decreasing burst rate with accretion rate; however, the argument for the mechanism we suggest could be behind this phenomenon relies mostly only on the fact that there is a dependence of the burst rate on a function $\bar{g}$, which is greater at the pole than at the equator.

The parameters α and β in Equation (3) depend on the burning regime under consideration. α clearly describes the dependence on accretion rate, while β is related to how the ignition depth depends on the local effective gravity and on mixing, which in turn are affected by the spin of the star and the colatitude θ, as noted above. In the most relevant cases, theory predicts α to be positive, which is also what intuition would predict: the faster matter is accreted on the star, the faster the critical conditions are reached for ignition. However, as already mentioned, many sources show a complexity of different behaviors, most importantly showing α apparently becoming negative (burst rate decreasing) after some accretion rate $\dot{M}_{\rm tot}$.

Previously, it was tentatively suggested that a possible reason for that is a change in accretion geometry that leads to the local accretion rate $\dot{m}$ decreasing while the global accretion rate $\dot{M}_{\rm tot}$ increases (see Bildsten 2000; Strohmayer & Bildsten 2006 and references therein), but exactly how this would happen was not clear. Narayan & Heyl (2003) and Cooper & Narayan (2007a) advocated instead a switch to their delayed mixed-burst regime. We provide a different explanation: the dimensionality of the problem is the key.

Most of the burning physics theory is obtained with 1D simulations, where the one dimension is the radial direction. Although this approach is extremely valuable, it does not take into account the fact that the surface of the star adds two extra dimensions, namely θ and ϕ, where the conditions are different even for a single star. The role of $\bar{g}$ in Equation (3) is then this: to incorporate the effects of the second dimension θ. $\bar{g}$ allows us to take into account the fact that at *different* colatitudes θ of a *spinning* NS, the burst rate given by the *same* physics will be *different* (basically due to the different centrifugal force or different mixing). The importance of this effect is given by the power β. It is difficult to find the β associated with the different theoretical works in the literature, since this aspect is often neglected and the ignition depth and its dependence on gravity and mixing are always reported vaguely, if at all. However, we can extract it, for example, from the calculations in Bildsten (1998) or Piro & Bildsten (2007). It can be seen that β is expected to be negative in the first case and positive in the second (see Sections 2 and 4 for more details).

So, how does this imply that above some critical $\dot{M}_{\rm tot}$ the burst rate should decrease? The last ingredient to provide the answer is the stabilization of burning. We show in Section 2 that bursting is possible at any colatitude θ (this was also recognized by Cooper & Narayan 2007a) provided that

$$\dot{m}_{\rm l}\bar{g}^{\gamma_{\rm l}} \leqslant N(\nu)\dot{M}_{\rm tot} = \dot{m}_{\rm p} \leqslant \dot{m}_{\rm h}\bar{g}^{\gamma_{\rm h}}, \tag{5}$$

where $\dot{m}_{\rm l}$ and $\dot{m}_{\rm h}$ are values dependent on the burning regime (Equation (18) and see Section 4 for an example). $\dot{m}_{\rm l}\bar{g}^{\gamma_{\rm l}}$ is the condition for the onset of bursts,[7] and $\dot{m}_{\rm h}\bar{g}^{\gamma_{\rm h}}$ is the condition for stabilization. As for β, $\gamma_{\rm l}$ and $\gamma_{\rm h}$ are related to the ignition depth and its dependence on the local effective gravity or mixing. Once again, it is difficult to obtain values of $\gamma_{\rm h}$ from the literature, but again we can infer its value for the cases treated by Bildsten (1998), where $\gamma_{\rm h} > 0$, or by Piro & Bildsten (2007), where $\gamma_{\rm h} < 0$. Note, however, that there is uncertainty around these values (see Section 4).

The explanation we suggest for the decreasing burst rate then goes as follows (see Figure 1 for a sketch). Let us consider the case $\beta < 0$, $\gamma_{\rm h} > 0$. Initially, the most probable ignition location is the equator, point A in Figure 1, because $\beta < 0$, $\bar{g}(\theta = \pi/2) < \bar{g}(\theta = 0)$, and this makes the rate at the equator the highest, Equation (3). With increasing $\dot{M}_{\rm tot}$, the most probable ignition site will remain on the equator, until the condition given by Equation (5) is broken (point B). In the range $\overline{\rm AB}$ of the accretion rate, the burst rate should be increasing as $\dot{M}_{\rm tot}^{\alpha}$ because the factor $\bar{g}^{\beta}$ in Equation (3) will not change. The fact that ignition stays on the equator depends on the fact that $\beta < 0$ (see Section 3 for further details and more possibilities). After point B, while the accretion rate $\dot{M}_{\rm tot}$ increases, the most probable ignition colatitude moves toward the pole, while the part near the equator should be burning

[7] The limit for the onset of the bursts of a specific burning regime should be thought more accurately as the limit when the burst rate of that specific regime becomes faster than the rate of the other regimes.

stably. When the pole becomes the most probable location, point C, the whole star should be burning stably and the bursts should disappear. In the range $\overline{\mathrm{BC}}$, the rate of the bursts will go as

$$\bar{\mathcal{R}} \propto \dot{M}_{\rm tot}^{\alpha+\beta/\gamma_{\rm h}}. \quad (6)$$

Depending on the sign of $\alpha + \beta/\gamma_{\rm h}$, the burst rate may actually decrease.

Note that *this condition is NOT in contradiction with the theoretical results of simulations that give a consistently increasing bursting rate as a function of* $\dot{M}_{\rm tot}$. As can be seen in Figure 1, at a fixed colatitude, $\bar{g}$ is a constant and the rate is increasing as a function of $\dot{M}_{\rm tot}$, but the dependence of ignition depth and burst rate on local position, measured by $\bar{g}^{\beta}$, makes the normalization factor in Equation (3) different at different colatitudes. The normalization is higher at the equator (if $\beta < 0$), so that the overall burst rate (normalization) near the pole can be significantly lower than at the equator.

If the "speed" in terms of $\dot{M}_{\rm tot}$ at which the ignition moves polewards is fast enough, the increase in burst rate due to $\dot{M}_{\rm tot}^{\alpha}$ will not be able to compensate for the initial deficit due to the normalization factor $\bar{g}^{\beta}$, and the burst rate will decrease. The "speed" at which the ignition moves polewards can be thought of as $\Delta\theta/\Delta\dot{M}_{\rm tot}$ or, more conveniently, $\Delta \ln \bar{g}/\Delta \ln \dot{M}_{\rm tot} = 1/\gamma_{\rm h}$; see Equations (5) and (36). A small $\gamma_{\rm h}$ leads to a high "speed" and decreasing burst rate, Case 2 in Figure 1. A high $\gamma_{\rm h}$ gives a slow "speed" and the increasing $\dot{M}_{\rm tot}^{\alpha}$ is able to cover the gap due to the normalization factor $\bar{g}^{\beta}$ and the observed burst rate will increase. We discuss more the role of α, β, and γ in Section 5.

Finally, note that the fact that the ignition moves off its initial site due to stabilization may also explain why bursts at a high accretion rate seem to be less energetic (van Paradijs et al. 1988). A smaller fraction of the star surface would be burning efficiently, since part of the fuel in the stabilized regions will have been spent in stable burning.[8] In the case of equatorial ignition, this very same mechanism may help explain why bursts seem to stabilize before the expected $\dot{M}_{\rm tot}$: the theoretical $\dot{M}_{\rm tot}$ from the 1D multizone simulations is the one corresponding to conditions at the pole, point C, since corrections due to rotations are absent there. However, at that point, the bursts may have become too weak and rare to be detected.

2. The Relation Among Bursting Rate, Accretion, and Spin Frequency

We begin by generalizing and extending the approach of Cooper & Narayan (2007a). Thus, we initially present results regarding the local effective gravity. In Section 3.1, we argue that mixing can have effects on the burst rate that are formally very similar to the effective gravity, even though of different magnitude. Mixing has not been explored as thoroughly as gravity. The latter offers therefore a more solid ground for beginning this presentation. The burning rate of a specific regime is generally described as a function of effective gravity $g_{\rm eff}(\theta, \nu)$ and local accretion rate $\dot{m}(\theta, \nu)$ (where ν is the spin frequency and θ is the colatitude measured from the north pole; see, for example, Bildsten 1998, 2000). Without considering general relativistic corrections,[9] $g_{\rm eff}$ is written

$$g_{\rm eff} = g - \Omega^2 R_\star \sin\theta^2, \quad (7)$$

where Ω is the angular velocity of the star ($\Omega = 2\pi\nu$) and $R_\star$ is the radius of the star. If we take $g_{\rm eff,\,p} = g = GM/R_\star^2$, we can write

$$g_{\rm eff} = g_{\rm eff,\,p}\left[1 - \left(\frac{\nu}{\nu_{\rm k}}\right)^2 \sin^2\theta\right], \quad (8)$$

where we have introduced the Keplerian frequency $\nu_{\rm k} = \sqrt{GM/R_\star^3}/2\pi$, G is the gravitational constant, and M is the mass of the star. We will write $g_{\rm eff} = g_{\rm eff,\,p}\bar{g}(\theta, \nu)$ for later convenience, so that

$$\bar{g} = 1 - \left(\frac{\nu}{\nu_{\rm k}}\right)^2 \sin^2\theta. \quad (9)$$

$\bar{g}$ depends not only on the spin and colatitude, but also on the mass and radius of the star through $\nu_{\rm k}$. It is the ratio $g_{\rm eff}(\theta, \nu)/g_{\rm eff,\,p}$ and it measures the modification to local gravity due to rotation with respect to a nonrotating star. Presently, it has to be interpreted as a function of position θ (and ν).

We also introduce the number ϵ, which is $\bar{g}$ evaluated at the equator,

$$\epsilon = \bar{g}(\pi/2, \nu) = 1 - (\nu/\nu_{\rm k})^2, \quad (10)$$

so that $\epsilon \leqslant \bar{g}(\theta, \nu) \leqslant 1$. ϵ is a quantity characteristic of each specific NS, combining the spin frequency, mass, and radius of the star. It is equal to 1 for nonrotating stars and equal to 0 for stars rotating at the Keplerian frequency. This latter limit is nonphysical because the star would not be bound, at least at the equator.

Assuming that the accreted material spreads rapidly over the surface, the local accretion rate $\dot{m}(\theta, \nu)$ at a specific colatitude is related to the local accretion rate at the pole $\dot{m}_{\rm p}$ through (Cooper & Narayan 2007a)

$$\dot{m}(\theta, \nu) = \dot{m}_{\rm p} g_{\rm eff,\,p} g_{\rm eff}(\theta, \nu)^{-1} = \dot{m}_{\rm p}\bar{g}(\theta, \nu)^{-1}. \quad (11)$$

We note that the local accretion rate at the pole can be related to the global accretion rate $\dot{M}_{\rm tot}$, the total amount of mass accreted per unit time as measured near the star, or to the surface-averaged local accretion rate $\dot{m}_{\rm av}$ as follows.

$4\pi R_\star^2 \dot{m}_{\rm av} = \dot{M}_{\rm tot} = \int \dot{m}(\theta, \nu) R_\star^2 \sin\theta \mathrm{d}\theta\mathrm{d}\phi$, where the integral is extended over the whole surface (assumed to be of spherical shape for simplicity and consistency with Equation (7)).[10] With Equations (9) and (11), this leads to $\dot{m}_{\rm av} = \dot{m}_{\rm p}/2\int \bar{g}(\theta, \nu)^{-1} \sin\theta \mathrm{d}\theta$, where the integral in ϕ yields 2π

[8] Of course, this is similar to the suggestion of Narayan & Heyl (2003), but here the origin of the stable burning is not the delayed mixed-burst regime, it is the competition between β and $\gamma_{\rm h}$ in the power of Equation (6). In this sense, the explanation is more similar to Bildsten (2000) even though we do not invoke any strongly changing accretion geometry.

[9] For the effects of general relativity, see AlGendy & Morsink (2014) and Section 5.

[10] If we were to include the effects of oblateness, the integral would be $\dot{M}_{\rm tot} = \int \dot{m}(\theta, \nu) R_\star^2 [1 + f^2(\theta)]^{1/2} \sin\theta \mathrm{d}\theta\mathrm{d}\phi$, where $f(\theta) = (\mathrm{d}R_\star/\mathrm{d}\theta)/R_\star$ and $R_\star$ is a function of θ only. This effect should be relevant only for very fast rotating stars ($\nu/\nu_{\rm k} \gtrsim 0.3$; AlGendy & Morsink 2014), unless general relativity effects are taken into account.

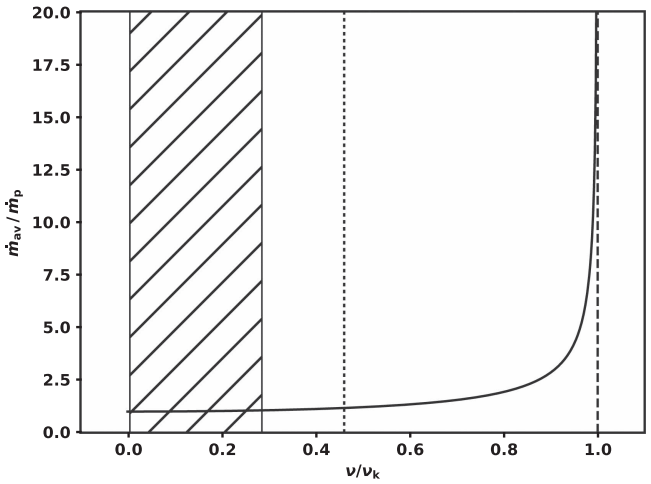

Figure 2. Relation between the observed, average accretion rate $\dot{m}_{av}$ and the local accretion rate at the pole $\dot{m}_p$. See Equation (12) and note that $\nu/\nu_k = \sqrt{1-\epsilon}$. The divergence of the ratio $\dot{m}_{av}/\dot{m}_p$ when $\nu = \nu_k$, the vertical asymptote (shown by the dashed line), is due to the fact that for a star rotating at the Keplerian frequency, the local accretion should be 0. This plot is general, and as a specific example, the dotted line indicates the position of a star of $M = 1.4\,M_\odot$ and $R_\star = 10$ km spinning at 10^3 Hz. The hatched region indicates the range of the known bursters: 11 Hz (Altamirano et al. 2010) to 619 Hz (Hartman et al. 2003).

since $\bar{g}$ does not depend on ϕ. After some algebra, the result is

$$\frac{\dot{M}_{tot}}{4\pi R_\star^2} = \dot{m}_{av} = \dot{m}_p \frac{\arctan\sqrt{(1-\epsilon)/\epsilon}}{\sqrt{\epsilon(1-\epsilon)}}. \quad (12)$$

$\epsilon = 0$ is not admissible and for $\epsilon \to 1$, $\dot{m}_p \to \dot{m}_{av}$. The mapping between $\dot{m}(\theta, \nu)$, $\dot{m}_p$, and $\dot{m}_{av}$ should be taken into account when comparing to observations, since observations are usually stated in terms of $\dot{M}_{tot}$ or $\dot{m}_{av}$, while theoretical models prefer the use of $\dot{m}(\theta, \nu)$. Equations (11) and (12) show how the relation between these quantities depends on the rotation frequency and the mass and radius of each star and is therefore different for different systems (see also Figure 2). However, for a star of mass $M_\star = 1.4\,M_\odot$ and $R_\star = 10$ km rotating at $\nu = 10^3$ Hz ($\nu/\nu_k \approx 0.43$, $\epsilon \approx 0.82$), the correction due to Equation (12) is only 1.14, so that this correction becomes important only for very rapidly rotating systems.

Analytical calculations show that the ignition depth y_{ign} (the column density in g cm^{-2} at which ignition takes place) can be expressed as a function of local mass accretion rate, local gravity, and the properties of the burning regime under consideration, and this is confirmed by direct numerical experiments (see Fujimoto et al. 1981; Bildsten 1998, and also Section 4). In general, expressions for the ignition temperature and depth can be estimated by combining the equations for the temperature profile across one column of fluid, obtained, for example, under the assumption of constant flux, with the conditions for unstable burning and/or depletion of a specific species (Fujimoto et al. 1981; Bildsten 1998). The flux depends on the burning regime or on extra heat sources, usually proportional to the accretion rate, like gravitational energy release or extra nuclear reactions at the bottom of the ocean. The conditions for instability are obtained by comparing the energy release rate due to the burning and cooling rate. Gravity enters the equations also through the equation of state of the burning fluid and the relation between pressure P and column depth: $P = y g_{eff}$. Then, the burst recurrence time can be expressed as the time it takes for accreted fluid to reach the ignition depth, $t_{rec} = y_{ign}/\dot{m}(\theta, \nu)$ (Bildsten 1998; Cooper & Narayan 2007a), and therefore we can write (see Section 4 for an explicit example)

$$t_{rec} \propto \dot{m}(\theta, \nu)^{-A}\, g_{eff}(\theta, \nu)^{-B}. \quad (13)$$

This expression could be used also to fit measurements from numerical experiments, therefore making it even more generally useful.

The bursting rate $\mathcal{R}$ is the inverse of the recurrence time, which leads to

$$\mathcal{R} \propto \dot{m}(\theta, \nu)^{A}\, g_{eff}(\theta, \nu)^{B}. \quad (14)$$

This can be rewritten as

$$\mathcal{R} = \bar{\mathcal{R}} \dot{m}(\theta, \nu)^{A}\, \bar{g}(\theta, \nu)^{B}, \quad (15)$$

where $\bar{\mathcal{R}}$ is a pseudo-constant that includes dependence on the mass and radius through $g_{eff,\,p} = GM/R_\star^2$ and physical parameters like the fluid composition and conductivity (see the example of Section 4, where we apply this to Equations (20) and (32) in Bildsten 1998, and remember that $\mathcal{R} = \dot{m}(\theta, \nu)/y_{ign}$). Using Equation (11), we can write

$$\mathcal{R} = \bar{\mathcal{R}} \dot{m}_p^{\alpha}\, \bar{g}^{\beta}, \quad (16)$$

where $\alpha = A$, $\beta = B - A$. In order to avoid cumbersome notation, we dropped the explicit dependence over θ and ν from $\bar{g}$, but that should be kept in mind since the role of $\bar{g}$ is to track the colatitude.

Typically, the bursting rate of a specific burning regime is only valid within an interval of local mass accretion rate, outside of which either the burning is stable or the burst rate of another regime is higher. The limits for stability set conditions on the burning temperature which, being found in a similar way to y_{ign}, can be expressed in terms of $\dot{m}$ and g_{eff} (see, for example, the derivation of Equations (24)–(26) or (36) of Bildsten 1998). The precedence of one regime over another is mainly set by comparing the column depth y_{ign} at which different regimes ignite and checking which one is smaller; once again, these conditions involve $\dot{m}$ and g_{eff} (e.g., Equation (35) of Bildsten 1998; Cooper & Narayan 2007a). As a consequence, these limits are quite generally of the form

$$\dot{m}_l \bar{g}^{\Gamma_l} \leqslant \dot{m}(\theta, \nu) \leqslant \dot{m}_h \bar{g}^{\Gamma_h}, \quad (17)$$

where $\dot{m}_l$ and $\dot{m}_h$ are again pseudo-constants that hide the dependence on physical parameters in the same way as $\bar{\mathcal{R}}$. The Γs are parameters that depend on the burning regimes and Γ_l need not necessarily be equal to Γ_h (see an example in Section 4). As for the burst recurrence time, these expressions could be used to fit the results from numerical simulations, thus providing a useful general form.

Thanks to Equation (11), these constraints can again be written for convenience as

$$\dot{m}_l \bar{g}^{\gamma_l} \leqslant \dot{m}_p \leqslant \dot{m}_h \bar{g}^{\gamma_h}, \quad (18)$$

where $\gamma_* = \Gamma_* + 1$. Forms (16) and (18) are preferable over (15) and (17), respectively, because they express the two conditions in such a way that the dependence over θ and ν (or ϵ) is only present through $\bar{g}$ and clearly separated from the dependence on the accretion rate, which is parametrized by $\dot{m}_p$.

$\dot{m}_{\rm p}$ has to be interpreted as a parameter that acts as a proxy for the observational information $\dot{m}_{\rm av}$ ($\dot{M}_{\rm tot}$), with the link being provided by Equation (12). In principle, Equations (16) and (18) could be expressed directly in terms of $\dot{m}_{\rm av}$ and ν (or ϵ), but that would make the following equations even more cumbersome.

Finally, a star can experience different dominant burning regimes, so we shall write in general

$$\mathcal{R}_i = \bar{\mathcal{R}}_i \dot{m}_{\rm p}^{\alpha_i}\, \bar{g}^{\beta_i} \tag{19}$$

and

$$\dot{m}_i \bar{g}^{\gamma_i} \leqslant \dot{m}_{\rm p} \leqslant \dot{m}_{i+1} \bar{g}^{\gamma_{i+1}}, \tag{20}$$

where the index i indicates the burning regime. The critical accretion rate $\dot{m}_{i+1}\bar{g}^{\gamma_{i+1}}$ is also the lower limit of the rate $\mathcal{R}_{i+1}$, etc.

The last quantities we need to define are the burst ignition rate evaluated at the two $\dot{m}_{\rm p}$ extremes of applicability:

$$\mathcal{R}_{i,i} = \mathcal{R}_i|_{\dot{m}_{\rm p}=\dot{m}_i\bar{g}^{\gamma_i}} = \bar{\mathcal{R}}_i \dot{m}_i^{\alpha_i}\, \bar{g}^{\delta_{i,i}}, \tag{21}$$

$$\mathcal{R}_{i,i+1} = \mathcal{R}_i|_{\dot{m}_{\rm p}=\dot{m}_{i+1}\bar{g}^{\gamma_{i+1}}} = \bar{\mathcal{R}}_i \dot{m}_{i+1}^{\alpha_i}\, \bar{g}^{\delta_{i,i+1}}, \tag{22}$$

where

$$\delta_{i,i} = \alpha_i\gamma_i + \beta_i \tag{23}$$

and

$$\delta_{i,i+1} = \alpha_i\gamma_{i+1} + \beta_i \tag{24}$$

are useful shortening notations (note also that $\delta_{i,*} = A_i\Gamma_* + B_i$).

3. Where Does Ignition Take Place, Given a Specific $\dot{m}_{\rm p}$?

For a given star with a given gravity and spin frequency, ignition is to be expected at the colatitude where the rate is higher (Cooper & Narayan 2007a). Let us consider the regime i. The first question is whether at each colatitude the regime can be realized at all. From Equation (20), we can see that at each θ, we need $\dot{m}_i\bar{g}^{\gamma_i} \leqslant \dot{m}_{i+1}\bar{g}^{\gamma_{i+1}}$. Otherwise, the regime i would be skipped there in favor of the regime $i+1$ (or $i-1$). This translates into

$$\bar{g}^{(\gamma_i-\gamma_{i+1})} \leqslant \left(\frac{\dot{m}_{i+1}}{\dot{m}_i}\right). \tag{25}$$

It will be useful to define

$$\Delta\gamma_i = \gamma_i - \gamma_{i+1}\ (=\Gamma_i - \Gamma_{i+1}), \tag{26}$$

$$\mu_i = \frac{\dot{m}_{i+1}}{\dot{m}_i} (\geqslant 1), \tag{27}$$

and

$$\epsilon_i^\star = \mu_i^{1/\Delta\gamma_i}. \tag{28}$$

It is easy to see that Equation (25) is satisfied by

$$\epsilon \leqslant \bar{g} \leqslant 1 \text{ if } \Delta\gamma_i < 0\ \&\ \epsilon_i^\star < \epsilon \text{ or } \Delta\gamma_i \geqslant 0, \tag{29}$$

$$\epsilon_i^\star \leqslant \bar{g} \leqslant 1 \text{ if } \Delta\gamma_i < 0\ \&\ \epsilon_i^\star \geqslant \epsilon. \tag{30}$$

Note that Equations (29) and (30) show that $\epsilon_i^\star$ marks a critical value for ϵ, and therefore for ν, across which the behavior switches in the case of $\Delta\gamma_i < 0$. If μ_i would be allowed to be also $\mu_i < 1$, there would exist cases where the maximum possible $\bar{g}$ would be less than one, i.e., ignition may not reach the pole, in analogy to the cases where the minimum value is $\epsilon_i^\star$ and not ϵ (i.e., some midlatitude and not the equator). That $\mu_i < 1$ seems highly unlikely, and therefore we do not treat this extra possibility here; see, however, Appendix A. The colatitude $\theta_i^\star$, which corresponds to $\epsilon_i^\star$, is given by

$$\theta_i^\star = \arcsin\sqrt{\frac{1-\mu_i^{1/\Delta\gamma_i}}{1-\epsilon}}. \tag{31}$$

$\theta_i^\star$ is the solution of $1-(\nu/\nu_{\rm k})^2\sin^2\theta_i^\star = \bar{g}_i^\star = \epsilon_i^\star$ and corresponds to $\pi/2 - \lambda_{\rm ign}$ of Equation (8b) of Cooper & Narayan (2007a). There exists also the solution $\pi - \theta_i^\star$, but this is in the southern hemisphere. Since the northern and southern hemispheres are symmetrical, we consider only northern hemisphere solutions. The condition for the existence of $\theta_i^\star$, if $\mu_i \geqslant 1$, is the same as Equation (30).

Equations (29) and (30) establish the range of colatitudes (parametrized by $\bar{g}$) where bursts can happen. The next question is: at a given accretion rate, parametrized by $\dot{m}_{\rm p}$, where does ignition take place first among the allowed colatitudes? This question was addressed by Cooper & Narayan (2007a), and we present its generalization here.

3.1. Another Mechanism Affecting the Burst Rate: Mixing

This is a good place to introduce another physical mechanism that affects burst rate, regime switching, and stability. In our formalism, that means another form for $\bar{g}$. In the derivation so far, we have followed Cooper & Narayan (2007a) and used the effects of the centrifugal force on local gravity to identify a function $\bar{g}$ that would have the following properties: (1) depends on spin and latitude (being 1 at the pole and <1 at the equator) and (2) changes the local behavior of bursts. The centrifugal force case is more intuitive, being well-known from the literature. However, another mechanism that depends on spin and is known for affecting the burst behavior is mixing. Piro & Bildsten (2007) give analytical and linear stability analysis results about mixing, in particular mixing due to the effective viscosity resulting from the Tayler–Spruit dynamo (Spruit 1999, 2002). The authors found that the mixing was more effective for slowly rotating stars. Keek et al. (2009) performed more sophisticated, yet still 1D, numerical simulations showing that mixing could also be important for fast spins. They also found that mixing due to other, purely hydrodynamical effects could be important for high-enough spins. However, they did not provide analytical expressions.

The analytical formulae of Piro & Bildsten (2007) are particularly useful for this paper, since they express the burst rate as $\mathcal{R} \propto \dot{m}^\alpha \nu^{-\beta}$ and the limits for burning regimes as $\dot{m}_{\rm crit} \propto \nu^{-\gamma}$. These formulae are derived based on equations averaged over the surface, especially over θ, but some dependence over θ is to be expected in reality (see Fujimoto 1993; Spruit 2002). Finding the exact formulae is beyond the scope of this paper, even though it definitely warrants further work based on the conclusions of Section 5 (see also Section 1.1), where we suggest that they could provide an explanation for the decreasing burst rate.

We can speculate, however, just in order to give a concrete example of what we mean. The biggest difficulty is how to extend the formulae of Spruit (2002) and, Piro & Bildsten (2007) to the entire surface of the star, keeping the dependence

over θ explicit. Since the Tayler–Spruit dynamo depends on an external source to keep the shear in the vertical direction and this can be provided more easily near the equator by the accretion disk, the simplest possibility is to consider something like $\nu \sin\theta$. Note also that this formulation becomes unphysical, predicting infinite (or at least very high) rates for slow rotators. We can speculate on the existence of a limiting, perhaps very small, value $\nu_{\rm min}$ such that we can write, for example, $\mathcal{R} \propto (\nu_{\rm min} + \nu \sin\theta)^{-\beta} \propto (1 + \nu \sin\theta/\nu_{\rm min})^{-\beta}$. The exact form is not important here, but it should be investigated when seeking a more quantitative analysis, of course: we use this one only as an example. Then one can write

$$\bar{g}_{\rm m} = \left(1 + \frac{\nu \sin\theta}{\nu_{\rm min}}\right)^{-1}. \tag{32}$$

The reason for the negative power is that in this way $\bar{g}_{\rm m}$ will be 1 at the pole and take a value $\epsilon_{\rm m}$ at the equator, just like $\bar{g}$ of Equation (9). In this example, the value at the equator would be

$$\epsilon_{\rm m} = \left(1 + \frac{\nu}{\nu_{\rm min}}\right)^{-1} < 1, \tag{33}$$

again characteristic of each star. Finally, for a given $\epsilon_i^\star$, the corresponding colatitude would be

$$\theta^\star_{{\rm m},i} = \arcsin\frac{\epsilon_i^{\star -1} - 1}{\epsilon_{\rm m}{}^{-1} - 1}. \tag{34}$$

We no longer discuss this formulation because it is not the goal of this paper, but it is not unreasonable to think that a similar expression to Equation (32) actually takes place. From such a formula, definitions for $\epsilon_{\rm m}$ and $\theta^\star_{{\rm m},i}$ could be obtained as we did for our example.

As a final remark, we note that if the effects of mixing are taken into account, the full formulae should in principle still include the effects of gravity: $\mathcal{R} \propto \dot{m}_{\rm p}^{\alpha}\, \bar{g}^{\beta}\, \bar{g}_{\rm m}^{\beta_{\rm m}}$. However, since $g_{\rm eff}$ does not change much from pole to equator, the effects of mixing should be dominant, unless the dependence over gravity is much higher than presently understood. The change over gravity could thus be ignored. From now on, we will only write our discussion in terms of $\bar{g}$, ϵ, and $\theta_i^\star$. The same conclusions apply to the functions set by gravity and the centrifugal force as in Equations (9), (10), and (31) or to the functions set by mixing, as in our example Equations (32)–(34).

3.2. Ignition Latitude of Type I Bursts

In order to determine at which colatitude ignition is to be expected, we first need to know what is the range of allowed θ. While Equations (29) and (30) give the overall range for a given star and burning regime across all possible accretion rates, the actual range at a specific $\dot{m}_{\rm p}$ can be smaller. The condition that determines this range is given by Equation (20). Bursts take place only for values of $\dot{m}_{\rm p}$ such that this relation is satisfied by at least one of the overall allowed colatitudes.

Then, from Equation (20), we can define two functions that will bound the range of available $\bar{g}$:

$$\bar{g}_{i,{\rm l}} = \left(\frac{\dot{m}_{\rm p}}{\dot{m}_i}\right)^{1/\gamma_i} \tag{35}$$

$$\bar{g}_{i,{\rm h}} = \left(\frac{\dot{m}_{\rm p}}{\dot{m}_{i+1}}\right)^{1/\gamma_{i+1}}. \tag{36}$$

However, these functions can return values greater than 1 or smaller than ϵ (or $\epsilon_i^\star$), thus violating Equations (29) or (30). In general, the correct values to consider are

$$\bar{g}_{i,i} = \min\{\max[\bar{g}_{i,{\rm l}}, \epsilon\,(\text{or } \epsilon_i^\star)], 1\}, \tag{37}$$

$$\bar{g}_{i,i+1} = \min\{\max[\bar{g}_{i,{\rm h}}, \epsilon\,(\text{or } \epsilon_i^\star)], 1\}, \tag{38}$$

and the real ranges for the available values of $\bar{g}$ at a specific $\dot{m}_{\rm p}$ are given by

$$\bar{g}_{\rm min} = \min(\bar{g}_{i,i}, \bar{g}_{i,i+1}), \tag{39}$$

$$\bar{g}_{\rm max} = \max(\bar{g}_{i,i}, \bar{g}_{i,i+1}). \tag{40}$$

Figure 3 shows schematically the various configurations of the available ranges (gray areas) that can be found depending on the signs of γ_i and γ_{i+1}. Note that $\bar{g} = 1$ is the pole, $\bar{g} = \epsilon$ is the equator, and $\bar{g} = \epsilon_i^\star$ is somewhere in between. In the figure, the points A and B are given by (see Equations (35) and (36))

$$\ln \dot{m}_{\rm p,\,A} = \ln \dot{m}_i + \gamma_i \ln \epsilon\,(\text{or } \epsilon_i^\star), \tag{41}$$

$$\ln \dot{m}_{\rm p,\,B} = \ln \dot{m}_{i+1} + \gamma_{i+1} \ln \epsilon\,(\text{or } \epsilon_i^\star). \tag{42}$$

It is clear from the definition of $\epsilon_i^\star$, Equation (28), that in the case of Equation (30), the points A and B coincide. Points C and D correspond, respectively, to

$$\ln \dot{m}_{\rm p,\,C} = \ln \dot{m}_{i+1}, \tag{43}$$

$$\ln \dot{m}_{\rm p,\,D} = \ln \dot{m}_i. \tag{44}$$

Finally, from Equation (16), it is immediately seen that $\max(\mathcal{R}_i) = \bar{\mathcal{R}} \dot{m}_{\rm p}^{\alpha_i} \max(\bar{g}^{\beta_i})$, so that the answer to the question of where ignition takes place, given a specific $\dot{m}_{\rm p}$, is

$$\beta_i > 0 \quad \bar{g} = \bar{g}_{\rm max}, \tag{45}$$

$$\beta_i = 0 \quad \forall\, \bar{g}, \tag{46}$$

$$\beta_i < 0 \quad \bar{g} = \bar{g}_{\rm min}. \tag{47}$$

In Figure 3, the ignition colatitudes for the case $\beta_i > 0$ are shown by the red dashed segments, while for $\beta_i < 0$ the colatitudes are indicated by the solid blue segments. Basically, $\beta_i > 0$ traces the upper boundary and $\beta_i < 0$ the lower boundary of the allowed colatitudes. If $\beta_i = 0$, any colatitude in the gray areas is equally probable.

3.3. The Bursting Rate Evolution for a Single Source

From an observational point of view, it is interesting to have an idea of how the bursting rate would evolve within the allowed range of $\dot{m}_{\rm p}$ depending on the parameters α_i, β_i, and γ_i and γ_{i+1}. In order to study the burst rate evolution for a single source, the starting equation is once again Equation (16). In this section, we restrict ourselves to the more physical condition $\alpha_i > 0$; the other cases, being an easy extension of these calculations, are reported in Appendix B.

If $\beta_i = 0$, the bursting rate always grows as

$$\mathcal{R}_i = \bar{\mathcal{R}}_i \dot{m}_{\rm p}^{\alpha_i}, \tag{48}$$

and there is not much else to say. The behavior is more diverse when $\beta_i \neq 0$ and requires a more detailed analysis. This is simple now that we know the paths that the ignition colatitude

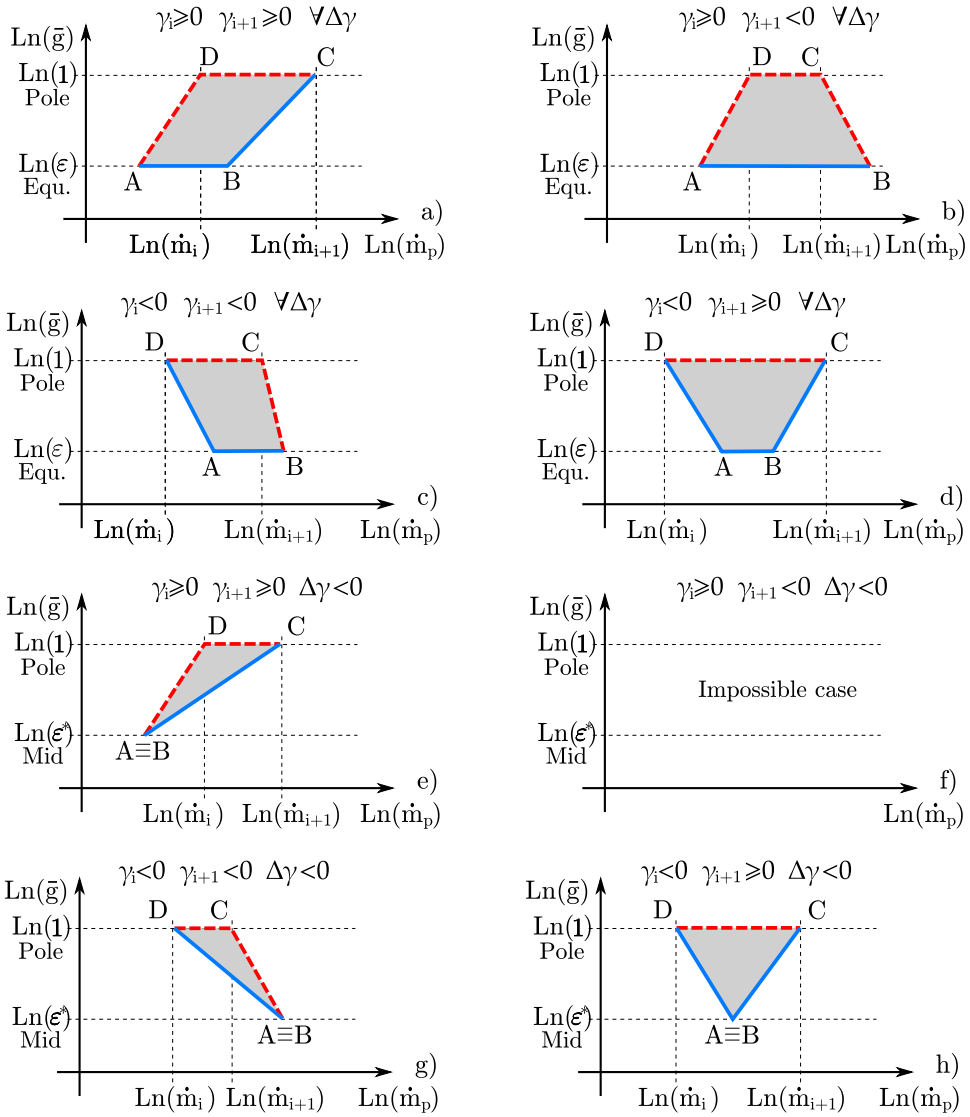

Figure 3. Simplified sketches showing the possible configurations of the allowed ranges of colatitudes where bursts can take place as a function of $\dot{m}_p$ for a single source and burning regime i. The ranges in colatitude are parametrized by $\bar{g}$ and are shown by the gray areas. The red dashed segments indicate the ignition colatitudes as a function of $\dot{m}_p$ when $\beta_i > 0$, and the solid blue segments indicate the ignition colatitudes when $\beta_i < 0$. In the case of $\beta_i = 0$, any colatitude in the gray areas is equally probable. Point A is the first $\dot{m}_p$ at which ignition is possible at the highest colatitude allowed, and B is the last one. D is the first $\dot{m}_p$ at which ignition is possible at the pole (the lowest colatitude allowed), and C is the last. Segments $\overline{\mathrm{AD}}$ correspond to the limit set by Equation (35), while segments $\overline{\mathrm{BC}}$ correspond to Equation (36). Cases (a)–(d): configurations for cases described by $\Delta\gamma_i < 0$ & $\epsilon_i^\star < \epsilon$ or $\Delta\gamma_i \geqslant 0$, Equation (29), where the overall minimum to $\bar{g}$ is ϵ (the equator). The differences are set by the sign of γ_i for $\overline{\mathrm{AD}}$ and γ_{i+1} for $\overline{\mathrm{BC}}$. In order, they are positive (or 0)–positive (0), positive (0)–negative, negative–negative, negative–positive (0). Note that the actual slopes are given by $1/\gamma_i$ and $1/\gamma_{i+1}$. In these cases, there is no implied relation between the magnitude of γ_i and γ_{i+1}, apart from the respective signs. For example, the first plot has $\overline{\mathrm{AD}}$ steeper than $\overline{\mathrm{BC}}$, but it could also be the contrary. The first three plots could even be triangles, with the top segment (the pole) collapsed to a point, but at least one $\dot{m}_p$ should be at the pole, due to the condition $\mu_i \geqslant 1$. Cases (e)–(h): same as cases (a)–(d), but for cases described by $\Delta\gamma_i < 0$ & $\epsilon_i^\star \geqslant \epsilon$, Equation (30), where the overall minimum to $\bar{g}$ is $\epsilon_i^\star$ and the points A and B coincide. Since $\Delta\gamma_i < 0$, $\gamma_{i+1} > \gamma_i$. Under this condition, the second case is impossible.

follows on the $\bar{g}$–$\dot{m}_p$ plane (Figure 3). The first step is to know the bursting rate $\mathcal{R}_i$ as a function of $\dot{m}_p$ on the various segments of the plots, then we can combine the different trends depending on which path is taken. The bursting rates are (using Equations (35) and (36))

$$\mathcal{R}_i = \frac{\bar{\mathcal{R}}_i}{\dot{m}_i^{\beta_i/\gamma_i}} \dot{m}_p^{\frac{\delta_{i,i}}{\gamma_i}} \text{ on } \overline{\mathrm{AD}}, \tag{49}$$

$$\mathcal{R}_i = \frac{\bar{\mathcal{R}}_i}{\dot{m}_i^{\beta_i/\gamma_{i+1}}} \dot{m}_p^{\frac{\delta_{i,i+1}}{\gamma_{i+1}}} \text{ on } \overline{\mathrm{BC}}, \tag{50}$$

$$\mathcal{R}_i = \bar{\mathcal{R}}_i \, \dot{m}_p^{\alpha_i} \text{ on } \overline{\mathrm{DC}}, \tag{51}$$

$$\mathcal{R}_i = \bar{\mathcal{R}}_i \epsilon^{\beta_i} \, \dot{m}_p^{\alpha_i} \text{ on } \overline{\mathrm{AB}}, \text{ when Equation (29) holds.} \tag{52}$$

It is seen from Equations (49) and (50) that when the ignition is moving between the pole and the equator (or the maximum colatitude allowed $\theta_i^\star$), the trend is set by the sign and magnitude of the ratios $\delta_{i,i}/\gamma_i$ and $\delta_{i,i+1}/\gamma_{i+1}$. In the spirit of Figure 3, we will not be concerned with the magnitude of these ratios, which can be determined by numerical simulations or fitted from observations, but we will study their sign.

The expected burst rate evolution for a single burning regime on a specific source for the cases $\beta_i \neq 0$ is shown in Figures 4 ($\beta_i < 0$) and 5 ($\beta_i > 0$). One thing to note is that, while the sign of $\delta_{i,i}/\gamma_i$ is not known in general, in the cases where it is

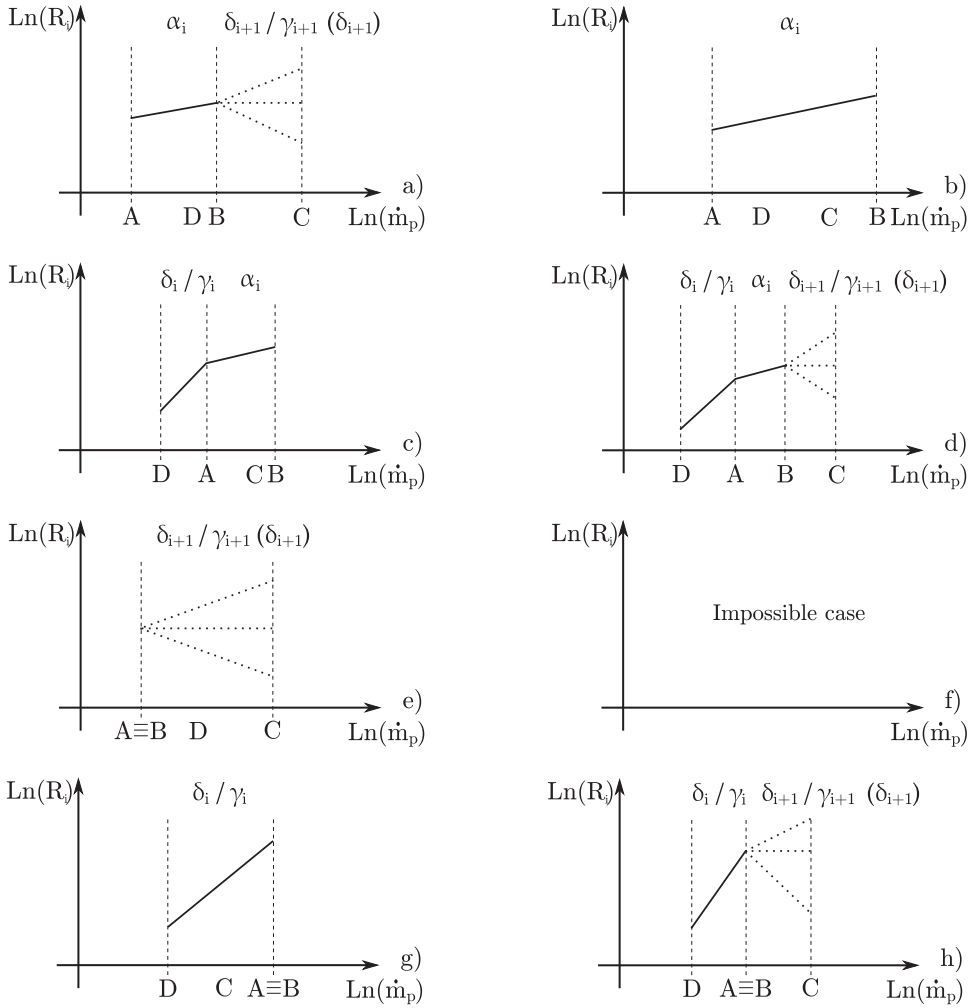

Figure 4. Bursting rate evolution of a single source as a function of $\dot{m}_p$, for cases when $\beta_i < 0$ and $\alpha_i > 0$: these correspond to the blue solid paths in Figure 3. The plots shown are in a one-to-one correspondence with the plots of Figure 3 and so are the indicated points A, B, C, and D. Indicated above each interval is the slope of the bursting rate. For the cases where the slope is $\delta_{i,i+1}/\gamma_{i+1}$, the sign of the slope is not determined, and we show the three possible cases (>0, $=0$, <0) using dotted lines. In parentheses, we indicate that the sign of the slope is dictated by the sign of $\delta_{i,i+1}$. On the other hand, it is known that $\delta_{i,i}/\gamma_i > \alpha_i > 0$ when $\delta_{i,i}/\gamma_i$ is the slope of the burst rate.

the slope of the function describing the bursting rate, we know it will be positive! These cases are plots (c), (d), (g), and (h) of Figure 4 and plots (a), (b), and (e) of Figure 5. The sign is known because $\delta_{i,i}/\gamma_i = \alpha_i + \beta_i/\gamma_i$ and for those cases, we know that $\beta_i/\gamma_i > 0$. That also implies that $\delta_{i,i}/\gamma_i > \alpha_i$, a fact that could be possibly detected by accurate enough observational campaigns. On the other hand, the same trick does not apply when we need to know the sign of $\delta_{i,i+1}/\gamma_{i+1}$: plots (a), (d), (e), and (h) in Figure 4 and plots (b), (c), and (g) in Figure 5. In those cases, $\beta_i/\gamma_{i+1} < 0$ and the sign of $\delta_{i,i+1}/\gamma_{i+1}$ depends on the difference $\alpha_i + \beta_i/\gamma_{i+1}$ or, equivalently, on the sign of $\delta_{i,i+1}$ when $\beta_i < 0$ (Figure 4) and the sign of $-\delta_{i,i+1}$ when $\beta_i > 0$ (Figure 5).

As an example, we describe now how to obtain plot (d) of Figure 4. We choose this example because it is one of the most complicated ones, not because we think this is a more likely one. For this we need to follow the blue solid line in the corresponding plot of Figure 3. Ignition starts at the pole (on D) and proceeds toward the equator as $\dot{m}_p$ increases ($\overline{AD}$). From Equation (49), we know that the rate is increasing $\propto \dot{m}_p^{\delta_{i,i}/\gamma_i}$. When ignition takes place on the equator ($\overline{AB}$), the bursting rate keeps increasing as $\dot{m}_p^{\alpha_i}$, but with a lower slope (Equation (52)), since $\delta_{i,i}/\gamma_i > \alpha_i$. Finally, for higher $\dot{m}_p$, ignition moves again toward the pole ($\overline{BC}$), and the bursting rate becomes $\propto \delta_{i,i+1}/\gamma_{i+1}$ (Equation (50)). It is impossible, on general grounds, to say if the rate will increase, remain constant, or decrease: this depends on the sign of $\delta_{i,i+1}$. The other plots are obtained in the same way. For example, plot (a) is very similar, only the segment $\overline{AD}$ is absent; in plot (e) the segment $\overline{AB}$ is also missing, since ignition starts off equator. The case of plot (b) from Figure 5 is very close in nature to the case of plot (d) of Figure 4, but reversed. Here, ignition is initially on the equator, A, and then moves toward the pole on $\overline{AD}$ (following the red path in Figure 3), the burst rate growing as $\dot{m}_p^{\delta_{i,i}/\gamma_i}$. While the flame ignites preferentially at the pole, on $\overline{DC}$, the rate grows as $\dot{m}_p^{\alpha}$ since the normalization factor due to $\bar{g}$ stays constant. Finally, after point C has been reached, ignition moves again toward the equator, with the burst rate evolving as $\dot{m}_p^{\delta_{i,i+1}/\gamma_{i+1}}$. If $\delta_{i,i+1}/\gamma_{i+1} < 0$, the burst rate will be observed to decrease. However, very differently from the cases when $\beta < 0$, the accretion rate at which the burst rate is seen to peak is constant: $\dot{m}_{i+1}$. Both in Figures 4 and 5 a negative $\delta_{i,i+1}/\gamma_{i+1}$

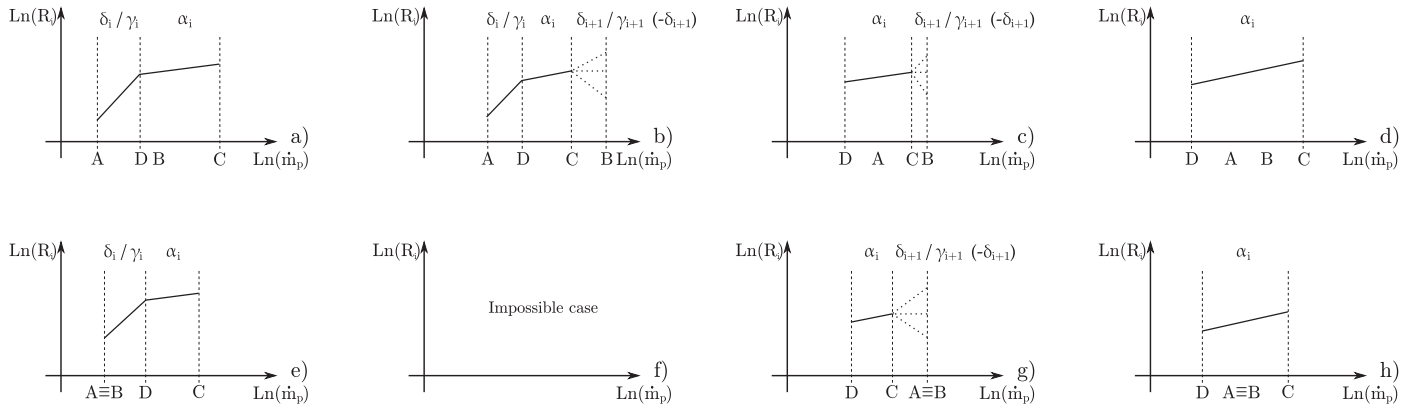

Figure 5. Same as Figure 4, but for cases when $\beta_i > 0$ and $\alpha_i > 0$, the red dashed paths of Figure 3. For the cases where the slope is $\delta_{i,i+1}/\gamma_{i+1}$, it is indicated in parentheses that the sign of the slope is dictated by $-\delta_{i,i+1}$. Also here $\delta_{i,i}/\gamma_i > \alpha_i > 0$, when $\delta_{i,i}/\gamma_i$ is the slope of the burst rate.

would result in the burst rate starting to decrease after some value of $\dot{m}_{\rm p}$ ($\dot{M}_{\rm tot}$).

4. Example Application

Here we provide an explicit example of the formalism of this paper, showing how the results of Bildsten (1998) and Piro & Bildsten (2007) for helium burning translate into the parameters α, β, etc. We start with the case of gravity, which is the most developed. In doing so, we repeat some of the formulae from the author.[11] This is also the regime initially described by Cooper & Narayan (2007a).

First, we show how to obtain the bursting rate parameters (see Equations (13)–(16)). In the case of ignition in a pure helium environment, the ignition depth is given by Equation (20) of Bildsten (1998):

$$y_{1,\rm ign} = 1.08 \times 10^{14} (Y\mu E_{18}\kappa)^{-2/5} \dot{m}^{-1/5} g_{\rm eff}^{-2/5} \ {\rm g\ cm^{-2}}, \quad (53)$$

where Y is the helium mass fraction, E_{18} is the energy released per unit mass by the burning in units of 10^{18} erg g^{-1}, and κ is the opacity in cm^2 g^{-1}.

$\mathcal{R} = \dot{m}(\theta, \nu)/y_{\rm ign}$, therefore

$$\mathcal{R}_1 = 9.28 \times 10^{-15} (Y\mu E_{18}\kappa)^{2/5} \dot{m}^{6/5} g_{\rm eff}^{2/5} \ {\rm Hz}. \quad (54)$$

Comparing this to Equations (14) and (15), and expanding $g_{\rm eff} = g_{\rm eff,\,p}\bar{g}$, it is seen that $A_1 = 6/5$, $B_1 = 2/5$, so that

$$\alpha_1 = 6/5 \text{ and } \beta_1 = -4/5. \quad (55)$$

The pseudo-constant $\bar{\mathcal{R}}_1 = 9.28 \times 10^{-15} (Y\mu E_{18}\kappa)^{2/5} g_{\rm eff,\,p}^{-4/5}$ Hz (g s^{-1} cm^{-2})$^{-6/5}$. It is evident how the properties of composition, opacity, burning regime, stellar mass, and radius are contained in $\bar{\mathcal{R}}$.

When helium burns in a mixed hydrogen–helium environment and flux from the bottom can be ignored (Equation (32) of Bildsten (1998)), the ignition depth is

$$y_{2,\rm ign} = 2.55 \times 10^{10} Y^{-1/3} Z_{\rm CNO}^{-5/18} \mu^{-2/9} \kappa^{-7/18} g_{\rm eff}^{-2/9} \ {\rm g\ cm^{-2}}; \quad (56)$$

here, $Z_{\rm CNO}$ is the metallicity, i.e., the mass fraction of carbon, nitrogen, and oxygen. Note that $y_{2,\rm ign}$ is independent of $\dot{m}$, even though this is not always the case (at high accretion rate and/or low metallicity; Bildsten 1998, Equation (37)). Therefore,

$$\mathcal{R}_2 = 3.92 \times 10^{-11} Y^{1/3} Z_{\rm CNO}^{5/18} \mu^{2/9} \kappa^{7/18} \dot{m} g_{\rm eff}^{2/9} \ {\rm Hz}, \quad (57)$$

so that $A_2 = 1$, $B_2 = 2/9$; then,

$$\alpha_2 = 1 \text{ and } \beta_2 = -7/9. \quad (58)$$

Furthermore, $\bar{\mathcal{R}}_2 = 3.92 \times 10^{-11} Y^{1/3} Z_{\rm CNO}^{5/18} \mu^{2/9} \kappa^{7/18} g_{\rm eff,\,p}^{2/9}$ Hz (g s^{-1} cm^{-2})$^{-1}$.

Second, we provide examples for the limits in the mass accretion rate, Equations (17) and (18), for the validity of the bursting rate of each of these burning regimes. In the case of pure helium bursts, the lower limit is set by the stability of the hydrogen burning, Equation (36) of Bildsten (1998), which otherwise would be bursting before helium could:

$$\dot{m}_{1,\rm l} = 4.18 \times 10^{-3} X^{-1} Z_{\rm CNO}^{1/2} \kappa^{-1/2} \ {\rm g\ s^{-1}\ cm^{-2}} \quad (59)$$

independent of gravity. The upper limit is set by the requirement that helium ignites at a depth where all hydrogen is depleted, Equation (35) of Bildsten (1998):

$$\dot{m}_{1,\rm h} = 2.32 \times 10^2 Z_{\rm CNO}^{13/18} X^{-1} \times Y^{-1/3} \mu^{-2/9} \kappa^{-7/18} g_{\rm eff}^{-2/9} \ {\rm g\ s^{-1}\ cm^{-2}}. \quad (60)$$

This means that $\dot{m}_1 = 4.18 \times 10^{-3}\ X^{-1} Z_{\rm CNO}^{1/2} \kappa^{-1}$ and $\dot{m}_2 = 2.32 \times 10^2 Z_{\rm CNO}^{13/18} X^{-1}\ Y^{-1/3} \mu^{-2/9} \kappa^{-7/18} g_{\rm eff,\,p}^{-2/9}$. Furthermore, $\Gamma_1 = 0$, $\Gamma_2 = -2/9$, and so

$$\gamma_1 = 1 \text{ and } \gamma_2 = 7/9. \quad (61)$$

Combining these with Equation (55), we have for Equations (23), (24), and (26)

$$\delta_{1,1} = 2/5, \quad (62)$$

$$\delta_{1,2} = 2/15, \quad (63)$$

$$\Delta\gamma_1 = 2/9. \quad (64)$$

For the case of helium ignition in a mixed hydrogen–helium environment, the lower limit is set by the upper limit of pure helium ignition, $\dot{m}_{2,\rm l} = \dot{m}_{1,\rm h}$. The upper limit is set by the stability of helium burning in this mixed composition

[11] The formulae will look slightly different because we rederived them in order to keep explicit all of the terms that involve the composition, we avoided rounding numbers in intermediate steps, and we applied no scaling to variables like $\dot{m}$ or $g_{\rm eff}$. We keep the opacity κ explicitly instead of inserting the electron-scattering formula $\kappa_{\rm es} = \sigma_{\rm Th}(1 + X)/(2m_{\rm p})$.

condition, Equation (24) of Bildsten (1998). This is

$$\dot{m}_{2,\mathrm{h}} = 1.79 \times 10^{-7} Y^{1/2} \mu^{1/2} E_{18}^{-3/4} \kappa^{-3/4} g_{\mathrm{eff}}^{1/2} \ \mathrm{g\ s^{-1}\ cm^{-2}}, \tag{65}$$

which leads to $\dot{m}_3 = 1.79 \times 10^{-7} Y^{1/2} \mu^{1/2} E_{18}^{-3/4} \kappa^{-3/4} g_{\mathrm{eff,\,p}}^{1/2}$, $\Gamma_3 = 1/2$, and

$$\gamma_3 = 3/2. \tag{66}$$

This implies, with Equation (58),

$$\delta_{2,2} = 0, \tag{67}$$

$$\delta_{2,3} = 13/18, \tag{68}$$

$$\Delta\gamma_2 = -13/18. \tag{69}$$

For an NS with $M = 1.4\,M_\odot$, $R_\star = 10$ km, accreting solar composition $X = 0.7$, $Y = 0.29$, $Z_{\mathrm{CNO}} = 0.01$, with the opacities reported by Bildsten (1998), we have $\bar{\mathcal{R}}_1 = 2.08 \times 10^{-8}$ Hz (g s^{-1} cm^{-2})$^{-6/5}$, $\bar{\mathcal{R}}_2 = 2.75 \times 10^{-9}$ Hz (g s^{-1} cm^{-2})$^{-1}$, $\dot{m}_1 = 6.69 \times 10^2$ g s^{-1} cm^{-2}, $\dot{m}_2 = 4.72 \times 10^3$ g s^{-1} cm^{-2}, and $\dot{m}_3 = 1.33 \times 10^5$ g s^{-1} cm^{-2} (this value is actually $\sim$1.5 times the local Eddington limit $\dot{m}_{\mathrm{edd}} = 2cm_{\mathrm{p}}/[\sigma_{\mathrm{Th}}(1+X)] = 8.88 \times 10^4$ g s^{-1} cm^{-2}),[12] and we have

$$\mathcal{R}_1 = 2.08 \times 10^{-8} \dot{m}^{6/5} \bar{g}^{-4/5} \ \mathrm{Hz}$$

$$\mathcal{R}_2 = 2.75 \times 10^{-9} \dot{m} \bar{g}^{-7/9} \ \mathrm{Hz}$$

$$\dot{m}_{1,\mathrm{l}} = 6.69 \times 10^2 \bar{g} \ \mathrm{g\ s^{-1}\ cm^{-2}}$$

$$\dot{m}_{1,\mathrm{h}} = \dot{m}_{2,\mathrm{l}} = 4.72 \times 10^3 \bar{g}^{7/9} \ \mathrm{g\ s^{-1}\ cm^{-2}}$$

$$\dot{m}_{2,\mathrm{h}} = 1.33 \times 10^5 \bar{g}^{3/2} \ \mathrm{g\ s^{-1}\ cm^{-2}}.$$

For the case of ignition in a pure helium environment, we have $\gamma_i = \gamma_1 > 0$, $\gamma_{i+1} = \gamma_2 > 0$, and $\Delta\gamma_1 > 0$, which corresponds to Equation (29) and to plot (a) of Figure 3. $\beta_1 < 0$, which according to Equation (47) means ignition will take place at $\bar{g}_{\mathrm{min}}$. Therefore, as $\dot{m}_{\mathrm{p}}$ increases, $\bar{g}_{\mathrm{ign}}$ will trace the lower boundary of the gray area (solid blue segments): starting at point A, ignition will be at the equator until the segment $\overline{\mathrm{BC}}$ begins, at which point ignition will move toward the pole following this segment. The case of helium ignition in a mixed hydrogen–helium environment is similar, having $\beta_2 < 0$, $\gamma_i = \gamma_2 > 0$, and $\gamma_{i+1} = \gamma_3 > 0$, but $\Delta\gamma_2 < 0$. In this case, the behavior is different for slow and fast rotators, where fast means
$\epsilon < \epsilon_2^\star = (1.33 \times 10^5/4.72 \times 10^3)^{1/-(13/18)} = 9.83 \times 10^{-3}$
or equivalently, $\nu > \nu_{\mathrm{k}}\sqrt{1-\epsilon_2^\star} = 9.95 \times 10^{-1}\nu_{\mathrm{k}}$. For slow rotators,[13] the evolution is again described by the lower boundary of plot (a) of Figure 3, but for fast rotators, the available ignition colatitudes are described by Equation (30) and plot (e) of Figure 3. For fast rotators, ignition begins off equator (at θ_2^*, $\bar{g} = \epsilon_2^\star$) on point A $\equiv$ B and moves polewards along the segment $\overline{\mathrm{BC}}$.

Since $\beta_1 < 0$ and $\beta_2 < 0$, the bursting rate evolution is described by the plots (a) and (e) of Figure 4. $\delta_{1,2} > 0$, so that plot (a) tells us that we would expect an always increasing bursting rate with increasing $\dot{m}_{\mathrm{p}}$ for pure helium burning, with a change of slope at some point. Since $\delta_{2,3} > 0$ also, plots (a) and (e) predict the same for bursts of helium ignition in a mixed hydrogen and helium environment, with the faster sources displaying one single slope. Since the maximum burst rate is attained at the pole, it is independent of the rotation of the star and so is the mass accretion rate of the peak, Equations (43) and (51).

We now move on to see how the results of Piro & Bildsten (2007) translate into our formalism. The main point to make is that the powers in the formulae of those authors should change signs, since we suggest having $\bar{g}_{\mathrm{m}}$ depend on the inverse of ν in order to have the minimum of $\bar{g}_{\mathrm{m}}$ at the equator. As for the burst rate, Equation (70) of Piro & Bildsten (2007) would read

$$\mathcal{R} \propto \dot{m}(\theta, \nu)^{1.25} \bar{g}_{\mathrm{m}}^{0.36}, \tag{70}$$

so that $\alpha = 1.25$ and $\beta_{\mathrm{m}} = 0.36$. The authors also report two limits for their regime of mixing modified helium burning:

$$\dot{m}(\theta, \nu)_{\mathrm{l}} \propto \bar{g}_{\mathrm{m}}^{-3}, \tag{71}$$

$$\dot{m}(\theta, \nu)_{\mathrm{h}} \propto \bar{g}_{\mathrm{m}}^{-0.62}, \tag{72}$$

so that $\gamma_{\mathrm{m,l}} = -3$ and $\gamma_{\mathrm{m,h}} = -0.62$. Note that also in the case of mixing, the analytical predictions would give a consistently increasing burst rate. $\beta_{\mathrm{m}} > 0$ and both $\gamma_{\mathrm{m},*} < 0$, so that the case is that described by plots (c) or (g) of Figures 3 and 5 ($\Delta\gamma_i < 0$). These cases allow for decreasing burst rate, but here $\delta_{i,i+1}/\gamma_{i+1} = 0.67 > 0$: the expected rate is increasing. However, once again, these are simplified analytical calculations and some differences with real burst physics are to be expected (see, e.g., Keek et al. 2009, who include a more elaborate version of the Tayler–Spruit dynamo and also find that at high spin hydrodynamical instabilities become efficient).

It is curious to note how both the case of Bildsten (1998) and the case of Piro & Bildsten (2007) do actually fall in the categories that would give decreasing a burst rate if the ratio $\delta_{i,i+1}/\gamma_{i+1}$ were negative. The values of α, β, and γ_* are uncertain enough that this could be happening in actuality. Between the two mechanisms mentioned above, we think mixing is the best candidate.

5. Summary and Discussion

5.1. The Role of Local Conditions

Wepresented simple analytical relations that would enable a comparison between models and observations. In Section 2, we began introducing the relation between the observed total mass accretion rate $\dot{M}_{\mathrm{tot}}$ (as measured near the star, via the average local accretion rate $\dot{m}_{\mathrm{av}}$, $\dot{M}_{\mathrm{tot}} = 4\pi R_\star^2 \dot{m}_{\mathrm{av}}$) and the local $\dot{m}_{\mathrm{p}}$ at the pole in Equation (12). This relation is used to facilitate the calculations since it allows us to compare one single observational piece of information, $\dot{M}_{\mathrm{tot}}$, to one single theoretical piece of information, $\dot{m}_{\mathrm{p}}$. However, as we noted, even up to $\nu = 10^3$ Hz (the fastest known NS spins at 716 Hz (Hessels et al. 2006), and the fastest burster spins at 620 Hz (Muno et al. 2002)), the difference between $\dot{m}_{\mathrm{av}}$ and $\dot{m}_{\mathrm{p}}$ is just of order 10%. Then, in Sections 2 and 3, we generalized the work of Cooper & Narayan (2007a) and presented a description of the burst rate $\mathcal{R}$ versus $\dot{m}_{\mathrm{p}}$. We parametrized the burning physics with various parameters ($\bar{g}$, α_i, β_i, γ_*, and $\dot{m}_*$). $\bar{g}$ is a function of the colatitude θ and the spin frequency ν. It is set by the dependence of the burning physics on local conditions. We discussed two possible mechanisms that may have an effect: local gravity, as explored by Cooper & Narayan (2007a), and mixing, as explored by Piro & Bildsten (2007). The

[12] This case is interesting because it shows that $\mu_i > 1$ even though the numerical coefficient of Equation (65) is smaller than the one of Equation (60).
[13] Note that in this case almost every NS would be a slow rotator, since the limit is very close to the mass-shedding limit.

two mechanisms establish different relations among ν, θ, and the burning physics, which are summarized by $\bar{g}^{\beta}$. In the case of the effective gravity, $\bar{g}$ is the ratio $g_{\rm eff}/g_{\rm eff,\,p}$, Equations (8) and (9). In the case of mixing, this dependence has not been worked out in full form yet (but see Spruit 1999, 2002; Piro & Bildsten 2007), and we just hint at a possibility in Equation (32).

The form of $\bar{g}$ is very important because we use it to express the colatitude of ignition once ν is fixed. While α_i expresses the dependence of the burst rate on the mass accretion $\dot{m}_{\rm p}$, β_i expresses the importance of each of the mechanisms that are at work in setting the burst rate, Equation (16). In the case of the changes to local gravity due to the centrifugal force, β is determined by the dependence of the ignition depth and the temperature profile of the column on gravity (Bildsten 1998). In the case of mixing, it is determined by the dependence of those very same quantities on the rotation–shear-induced mixing (Piro & Bildsten 2007). The $\dot{m}_*$ are the boundaries of the accretion rate where bursts can take place as calculated in the absence of rotation, e.g., at the pole; these boundaries at other colatitudes depend also on the local conditions via $\bar{g}^{\gamma_*}$, Equation (18). As can be seen, the local conditions, whether set by the effective gravity, mixing, or other mechanisms, are very important, because they control very strongly the evolution of the burst rate. In Section 3, we discussed the case $\alpha_i > 0$, i.e., when locally the burst rate increases with accretion rate. We provided summarizing formulae and plots for the ignition colatitude and burst rate as a function of $\dot{m}_{\rm p}$ ($\dot{M}_{\rm tot}$): Equations (45)–(52) and Figures 3–5. In the Appendices, we provide similar results for other, less likely cases.

Due to their nature, the equations were derived under somewhat simplified assumptions, which could be improved. First, general relativistic corrections to $g_{\rm eff}$ could be taken into account. AlGendy & Morsink (2014), for example, show that rotation introduces further terms to the ratio $g_{\rm eff}/g_{\rm eff,\,p}$ that we do not include in Equation (9). These terms depend on the oblateness of the star and the mass quadrupole moment. These corrections have a different form from Equation (9) and can be higher even for stars rotating at 500 Hz (AlGendy & Morsink 2014). Thus, they would change some of the quantitative conclusions drawn from the equations of this paper. The nature of the conclusions should not be affected. Second, the local accretion rate depends on ν and θ only through the effective gravity term, Equation (11). This may not be the case depending on the extent of the boundary layer (Bildsten 2000) or if some form of confinement is operating, for example due to magnetic fields. This may change Equation (11) and therefore most of the following equations. Third, there may even be a dependence on $\dot{M}_{\rm tot}$ of the extent in θ of the boundary layer or of the size of the accretion column in the case of strong magnetic fields: this would even make Equations (11) and (12) nonlinear in $\dot{M}_{\rm tot}$. Finally, extra heating in the upper layer where accretion takes place may affect the ignition depth, burst rate, and boundaries in the mass accretion rate as in Equations (16) and (18). This effect could arise from a magnetic hot spot or if some heating mechanism is at work at the accretion disk boundary layer (as suggested by Inogamov & Sunyaev 1999, 2010). These effects would introduce different dependencies on the spatial position (θ, ϕ) and, in the case of the boundary layer, also on ν; therefore, $\bar{g}$ would have a different form. Including these dependencies may contribute to further refining the equations presented here. We leave this for future work.

We continued in Section 4, presenting an example application that shows how the equations and plots of Section 3 and of the Appendices could be used, after the ν-dependent conversion between $\dot{M}_{\rm tot}$ and $\dot{m}_{\rm p}$ has been applied. We showed in a straightforward way that the dependencies predicted by theory (in this case the values of α_i, β_i, γ_* ,and $\dot{m}_*$ based on the simplified analytical calculations of Bildsten 1998 and Piro & Bildsten 2007) would not agree with observations, since they predict a consistently increasing burst rate versus $\dot{M}_{\rm tot}$, even taking into account the effects of local gravity and mixing.

5.2. A Mechanism for Decreasing Burst Rate

The second goal (and a very exciting conclusion) of this paper is a possible explanation that naturally accounts for two observational oddities: decreasing burst rate with increasing $\dot{M}_{\rm tot}$, and the weakness of the high $\dot{M}_{\rm tot}$ bursts. The decrease in burst rate after a certain accretion rate $\dot{M}_{\rm tot}$ is relatively common (see e.g., Cornelisse et al. 2003). The reason behind this decrease has been a mystery for many years. It has been explained either as a consequence of a switch to a burning regime with intrinsically decreasing burst rate, $\alpha < 0$ in our formalism (Narayan & Heyl 2003; Cooper & Narayan 2007a), or as a change in accretion geometry that changes the local $\dot{m}$ (see Bildsten 2000; Strohmayer & Bildsten 2006). We think we can explain it with the effect that the local conditions have on the burst rate, e.g., due to effective gravity or mixing. From the plots in Section 3 (Figures 4 and 5), it can be seen that it is actually possible to have a decreasing burst rate, even if $\alpha_i > 0$ locally all the time. The condition for this is that $\delta_{i,i+1}/\gamma_{i+1} = \alpha_i + \beta_i/\gamma_{i+1} < 0$. The physical meaning of this combination is as follows.

Consider a case with $\beta_i < 0$, $\gamma_i > 0$, and $\gamma_{i+1} > 0$; we will highlight the role of each parameter separately, starting with γ_{i+1} (see also Section 1.1 and Figure 1). The burst rate is given by Equation (16), $\mathcal{R} \propto \dot{m}_{\rm p}^{\alpha_i}\bar{g}^{\beta_i} \propto \dot{M}_{\rm tot}^{\alpha_i}\bar{g}^{\beta_i}$. The factor $\bar{g}^{\beta}$ sets the difference between the burst rate at the equator and the pole (and also all of the other colatitudes). Since $\bar{g}(\theta = \pi/2) < \bar{g}(\theta = 0)$ and $\beta_i < 0$, the burst rate at the equator is higher and the bursts initially ignite there. As long as the equator can burst, the rate in this phase will grow as $\dot{M}_{\rm tot}^{\alpha_i}$. When the equator stabilizes, the ignition site moves polewards at a "speed" $\Delta \ln \bar{g}/\Delta \ln \dot{M}_{\rm tot} = 1/\gamma_{i+1}$. It will reach the pole in $\Delta \ln \dot{M}_{\rm tot} = -\gamma_{i+1} \ln \epsilon$, where ϵ is $\bar{g}$ evaluated at the equator. The rate will be $\bar{\mathcal{R}} \propto \dot{M}_{\rm tot}^{\alpha_i+\beta_i/\gamma_{i+1}}$. If the ignition moves toward the pole in a range $\Delta \ln \dot{M}_{\rm tot}$ that is wide enough, and the growth of the burst rate due to $\dot{M}_{\rm tot}^{\alpha_i}$ is able to compensate the initial gap due to $\bar{g}^{\beta_i}$, then the burst rate will increase (large γ_{i+1}; Case 1 in Figure 1). If the ignition moves toward the pole in a range $\Delta \ln \dot{M}_{\rm tot}$ that is too narrow, then the increase of the burst rate due to $\dot{M}_{\rm tot}^{\alpha_i}$ will not be able to overcome the initial gap and the burst rate will decrease (small γ_{i+1}; Case 2 in Figure 1). If $\beta_i > 0$, the situation is analogous, with the pole and equator exchanging roles. This time the pole has the advantage; see, for example, plot (c) in Figure 5. When the ignition leaves the pole toward the equator on the segment $\overline{\rm BC}$, the growth in the burst rate due to $\dot{M}_{\rm tot}^{\alpha_i}$ can or cannot compensate the initial gap due to $\bar{g}^{\beta_i}$ depending on the value of the interval $\Delta \ln \dot{M}_{\rm tot} = \gamma_{i+1} \ln \epsilon$. Note that in the case where $\beta_i > 0$, we need $\gamma_{i+1} < 0$. The burst rate is of course $\propto \dot{M}_{\rm tot}^{\alpha_i+\beta_i/\gamma_{i+1}}$. In Figure 6, we describe how differences in β and α can have similar effects. In panel (a), we show the effect of β. β sets the gap between the burst rate at different

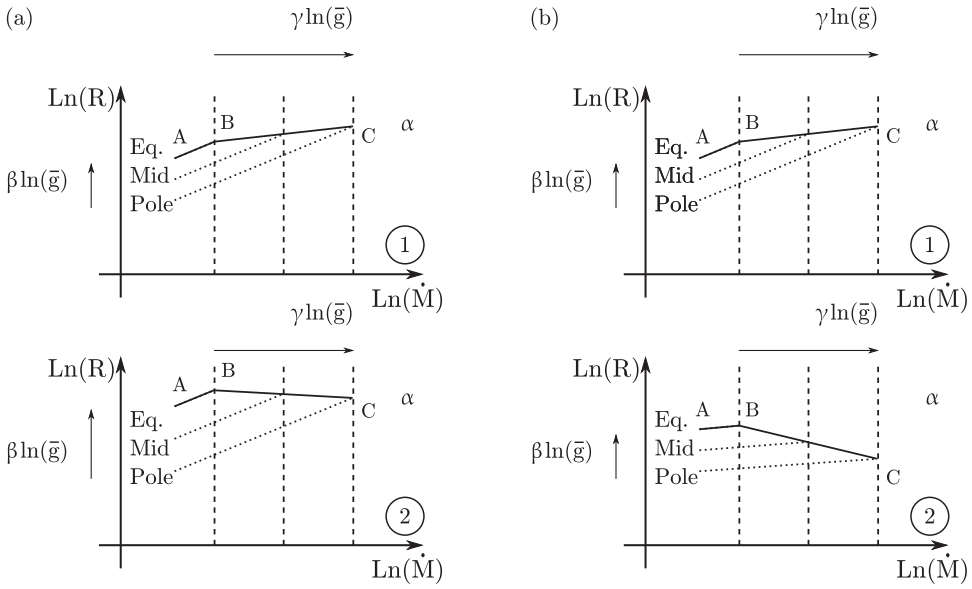

Figure 6. Same as Figure 1, but highlighting the effects of β, panel (a), and α, panel (b). Panel (a): at fixed α and γ_{i+1}, if $\beta < 0$ and $|\beta|$ is small, Case 1, then the increase in burst rate due to increasing $\dot{M}_{\rm tot}^{\alpha}$ can cover the gap due to the normalization factor $\bar{g}^{\beta}$, and the burst rate is seen to increase. When $|\beta|$ is large, Case 2, the gap is too wide and the increasing burst rate cannot compensate for it: the burst rate is seen to decrease. Panel (b): at fixed β and γ_{i+1}, if α is high enough, Case 1, then the burst rate keeps increasing also when the ignition moves off the equator. If α is low, Case 2, then the increasing $\dot{M}_{\rm tot}^{\alpha}$ cannot compensate for the normalization factor and the burst rate is seen to decrease. For both panels, in Case 1, $\delta_{i,i+1}/\gamma_{i+1} > 0$, and in Case 2, $\delta_{i,i+1}/\gamma_{i+1} < 0$.

colatitudes. If $\beta < 0$, the higher $|\beta|$, the higher this gap will be (since $\bar{g} \leqslant 1$). For high $|\beta|$, the increase in $\dot{M}_{\rm tot}^{\alpha}$ will not be able to compensate for the gap and the burst rate will decrease, Case 2. If $|\beta|$ is small enough, the gap can be covered and the burst rate will increase, Case 1. In panel (b) we show the role of α, which is apparent by now. If α is high enough, $\dot{M}_{\rm tot}^{\alpha}$ will be high and will be able to cover the gap due to the normalization factor $\bar{g}^{\beta}$, Case 1. Otherwise, the rate will be seen to decrease, Case 2. The physical meaning of the condition $\alpha_i + \beta_i/\gamma_{i+1} < 0$ is then this: that the resulting rate when ignition moves off the initially favored site is a competition between the increase in rate set by α_i and the initial gap set by β_i compensated by the "speed" $\Delta \ln \bar{g}/\Delta \ln \dot{M}_{\rm tot}$ set by $1/\gamma_{i+1}$.

This simple mechanism can explain quite naturally the decrease in burst rate with the initial gap in burst rate, the process of stabilization of the bursts, and the migration of the ignition to other colatitudes. It is also very appealing because it reconciles the observations with the time-dependent 1D simulations that predict a consistently increasing burst rate $\alpha_i > 0$. At the same time, since a smaller fraction of the star is available for the unstable burning of regime i, the rest of the star would be burning stably. The stable burning would reduce the available fuel for the spreading flame of the bursts after ignition took place, thus explaining the other observational feature: less energetic bursts (van Paradijs et al. 1988; Strohmayer & Bildsten 2006, and references therein). If this scenario is true, it may also have implications for all observational attempts at measuring the NS radius that exploit the bursts, since not all areas of the star may be emitting, at least not homogeneously. Furthermore, the decrease in burst rate and the weakening of the bursts would make them more difficult to detect before the theoretical limit is reached, and this, combined with other stabilizing effects (e.g., Keek et al. 2009), would give the impression of stabilization before the expected theoretical value of the accretion rate boundary.

The last sentence needs some refinement. We presented two cases where it is possible for the burst rate to decrease: $\beta < 0$, with bursts initially igniting on the equator, and $\beta > 0$, with bursts initially at the pole. The value of $\Delta \ln \dot{M}_{\rm tot}$ between the peak of the burst rate and the end of the bursts is $|\gamma_{i+1} \ln \epsilon|$ in both cases. This value depends on the spin of the star via ϵ. However, the value of $\dot{M}_{\rm tot,\ max}$ at which the peak is reached is different. In the case $\beta > 0$, the maximum is reached at the pole, point C, and $\dot{M}_{\rm tot,\ max} = N(\nu)\dot{m}_{i+1}$, Equation (2), is almost constant since $N(\nu)$ is very close to 1 for all known bursters, unless various effects (like the accretion processes discussed at the beginning of this section) contribute to make $N(\nu)$ a stronger function of ν. In the other case, $\beta < 0$, $\dot{M}_{\rm tot,\ max} = N(\nu)\dot{m}_{i+1}\epsilon^{\gamma_{i+1}}$. This value depends on the spin of the star more strongly, especially if ϵ is given by what we call $\epsilon_{\rm m}$: the value due to mixing. It is therefore easier to reconcile theory and observations if $\beta < 0$: the theoretical value for the quenching of the bursts may be when the bursts are already too rare and dim to be detectable above the fluctuating background accretion luminosity. The case $\beta > 0$ is still possible, of course, but this would require a very strong correction to our present understanding, since the value predicted by theory would then correspond to $\dot{M}_{\rm tot,\ max}$, which is much lower then current estimations. This latter case seems less likely.

We also mentioned cases where limits to $\bar{g}$ are set by $\epsilon_i^{\star}$, Equation (28) and Appendix A. These correspond to cases when $\mu_i \geqslant 1$ and $\Delta\gamma_i < 0$ (or when $\mu_i < 1$ and $\Delta\gamma_i > 0$, see Appendix A). They correspond to cases where the equator (or the pole) is always stable for slow rotators. It is interesting to note that $\dot{M}_{\rm tot}$, corresponding to $\epsilon_i^{\star}$, $\dot{M}_{\rm tot} = N(\nu)\dot{m}_{i+1}\epsilon_i^{\star\gamma_{i+1}}$, is almost a constant. That is because of the weak changes of $N(\nu)$ and the fact that $\dot{m}_{i+1}$, $\epsilon_i^{\star}$, and γ_{i+1} are constants depending only on the burning physical processes. This is a partial artifact of the cases we treated. $\epsilon_i^{\star}$ comes from equating $\dot{m}_i \bar{g}^{\gamma_i} = \dot{m}_{i+1}\bar{g}^{\gamma_{i+1}}$. The fact that ν and θ always appear together with the same form in the $\bar{g}$ (namely $\nu \sin\theta$) makes the equality one equation in one unknown, the unknown being $\nu \sin\theta$. Then, $\nu \sin\theta$ is fully determined and so are the $\bar{g}$, which in turn make $\dot{m}_{\rm p}$ fully

determined and constant. On the other hand, if the two $\bar{g}$ on the two sides of the equivalence were in fact different, most importantly depending differently onν and θ, something that would happen, for example, if different mechanisms were at work or if accretion physics were to change Equation (11) and the relation between $\dot{m}$ and $\dot{m}_{\rm p}$, then equating the two boundaries for regime i would provide one equation in two unknowns and therefore return a value for $\epsilon_i^\star$ and the corresponding $\dot{m}_{\rm p}$ that would depend explicitly on ν. This would also result in some $\dot{M}_{\rm tot,\ max}$ depending more strongly on ν.

Very preliminary analysis of observational data shows that the parameters β and γ_* would need to be very large to account for observations if only the effect of changing gravity is taken into account. This can be seen from the fact that the span in $\dot{m}_{\rm p}$ between the peak burst rate and the minimum is $\gamma_{\rm h} \ln \epsilon$. Even taking into account general relativistic effects, ϵ is still very close to 1 even for fast rotators and that makes the logarithm almost zero. On the other hand, when we considered mixing, we suggested that $\bar{g}_{\rm m}$ would be mostly proportional to ν, and so would be $\epsilon_{\rm m}$ (see Section 3.1). That can lead to much stronger effects. We do not study the exact form of $\bar{g}_{\rm m}$ in this work, but deem it a very worthy direction for research.

Finally, we want to add that any other mechanism could explain the decreasing burst rate if it would set a gap between the burst rate from different ignition locations and it would provide a means of moving the ignition between these sites fast enough so that the increase due to $\dot{M}_{\rm tot}^{\alpha}$ would not be able to compensate for the initial gap. We think that the local effective gravity and mixing are among the most natural of such mechanisms.

5.3. Future Perspectives

Ultimately, a joint effort of fitting to observations and running sets of numerical models varying both $\dot{m}$ and ν should provide a test of the idea described above and, if successful, our equations would provide the constraints that theory has to follow to reproduce the observations. The θ-dependent effects of mixing should be included self-consistently. We plan to perform a detailed comparison with observations in the future, but here we mention some considerations concerning the applications of Equation (16) when comparing to different sources. First of all, the importance of composition. We saw that composition is important because it determines the value of the coefficients $\bar{\mathcal{R}}_i$, $\dot{m}_i$ and $\dot{m}_{i+1}$. Lampe et al. (2016) showed that composition, even small variations in metallicity, will also change the values of the parameter α. It seems reasonable to expect that β and γ may also be affected to some degree and therefore values may be different from source to source. Piro & Bildsten (2007) and Keek et al. (2009) also stress the effects of mixing. Piro & Bildsten (2007) suggest that, to test the effects of spin at a first-order approximation, it would be sufficient to run simulations varying the mass fraction of helium. The work of Lampe et al. (2016) changed the composition (even if the fraction of helium was tied to that of the metallicity of the CNO species) for a part of the range suggested by Piro & Bildsten (2007). In Figure 1 of Lampe et al. (2016), it can be seen that indeed the burst stabilized at an appreciably different $\dot{m}$. Second, we want to point out that following the evolution of a single source, different burning regimes will be experienced and therefore changes in the parameters are to be expected when the burning regimes switch. For example, the phase when the burst rate decrease is observed could be described by the mechanism we propose during the burning of helium in a mixed hydrogen–helium environment followed by the regime of delayed mixed bursts described by Narayan & Heyl (2003) and Lampe et al. (2016), where $\alpha < 0$ at the very latest stages of the accretion rate. This regime happens for a very narrow range at high $\dot{M}_{\rm tot}$, before the bursts disappear. Even if this happens at too high $\dot{M}_{\rm tot}$ to explain the observed decrease in burst rate in all sources, it could still play a role in the very last stages of the decreasing burst rate determined by the mechanism we propose. Another example is what would happen when the switch is not between a burning regime and burst stability, but between the burning regime i and the burning regime $i+1$. Locally, the switch always happens when the burst rate of regime $i+1$ becomes faster than the rate of regime i. Suppose the switch from regime i to $i+1$ takes place initially at the equator, then the burst rate $i+1$ at the equator can be either faster or slower than the burst rate i at some other colatitude. If it is higher, then the switch will also take place from the point of view of the observer. If it is slower, then the burst rate will look like that of bursts of regime i for higher accretion rates until the burst rate of regime $i+1$ eventually overtake. In both cases, the flame of the bursts will meet different conditions across the surface of the star, giving, for example, light curves with mixed properties: these effects would need to be simulated with multidimensional simulations (see below) and studying a series of burning regimes would need the comparison of the compositions of the diagrams of Figures 3–5 to observations.

A striking feature of the relations in Section 3 is how the kind of expected behavior depends mostly on the sign of $\delta_{i,*}$ and the sign of the parameters γ_i, γ_{i+1}. In case of behavior switching, controlled once again by γ_i and γ_{i+1}, through $\Delta\gamma_i$, $\mu_i = \dot{m}_i/\dot{m}_{i+1}$ is also an important parameter. The role of $\delta_{i,*}$ is particularly informative: since $\delta_{i,*}$ combines both the contribution from the bursting rate, via α_i, β_i, and the boundaries in the mass accretion rate of a bursting regime, via γ_*, one cannot say that one of these aspects is much more important then the other. For example, both a small, positive γ_{i+1} or a strong, negative β_i would give a negative $\delta_{i,i+1}$. However, small or large is relative to the value of α_i. As a possibility, the values of γ_{i+1} and β_i required to explain the observations could be determined, respectively, by a weak dependence on $\bar{g}$ of the bound on accretion rate or a strong positive dependence on $\bar{g}$ of $y_{\rm ign}$, but there are, of course, other possible combinations. However, since all of these parameters, in one way or another, come from the ignition depth of a specific burning regime (see Section 2), and this in turn depends quite strongly on the energy release rate, this brings further evidence in support of the need that nuclear research has to focus on better understanding the reaction rates, which set the temperature of the burning region (Schatz 2011). Another important point to clarify, which also influences the ignition depth, is the origin and magnitude of extra heat sources due, for example, to the accretion process or further reactions in deeper layers as speculated for explaining superbursts or NS cooling behavior. The dependence of these factors on the local conditions at different colatitudes is key.

In an idealized procedure, one would have to input physical parameters in 1D simulations and then extract the exponents α_i, β_i, and γ_* and the masses $\dot{m}_*$ from the simulations changing the effective gravity $g_{\rm eff}$, the local accretion rate $\dot{m}$, and also the composition (see, for example, Lampe et al. 2016 and also Galloway et al. 2017), compare the results to the constraints obtained from the data (similar to those of Cornelisse et al. 2003, for example), introduce more refined physical processes, and then repeat the procedure until convergence. The value of α for helium burning from the literature and

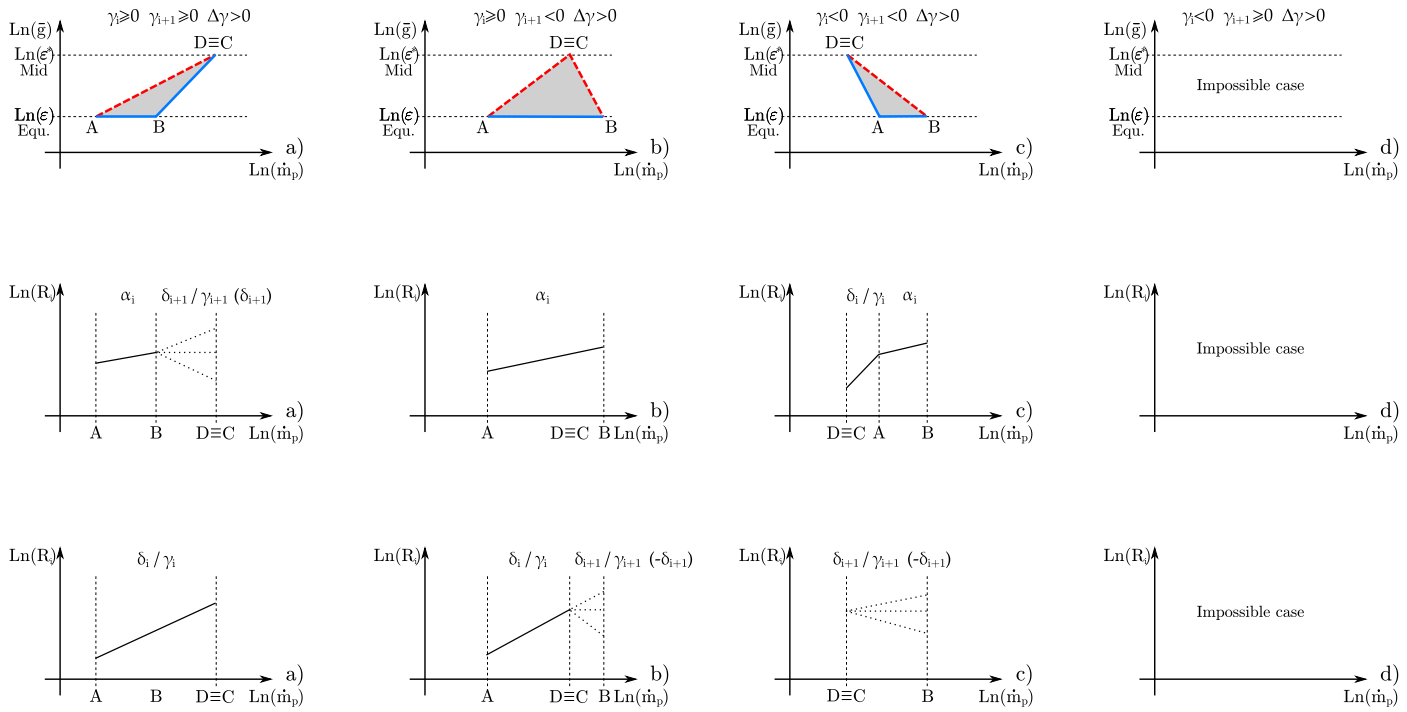

Figure 7. Upper panel: available colatitudes for different combinations of the sign of γ_i and γ_{i+1} as in Figure 3, but for the case $\mu_i < 1$. One difference is that the maximum available for $\bar{g}$ is $\epsilon_i^\star$. Also, the fourth case, $\gamma_i < 0$ and $\gamma_{i+1} > 0$ (or 0), is impossible due to the requirement $\Delta\gamma_i > 0$. The red dashed segments correspond to the paths followed by ignition when $\beta_i > 0$; the blue solid segments are the paths followed when $\beta_i < 0$. When $\beta_i = 0$, any colatitude in the gray areas is equiprobable. Middle panel: burst rate evolution when $\beta_i < 0$, corresponding to the blue solid paths in the upper panel. As in Figure 4, we know that $\delta_{i,i}/\gamma_i > \alpha_i > 0$ when it is the slope of the burst rate. The sign of $\delta_{i,i+1}/\gamma_{i+1}$ is not known when needed and the slope sign is determined by the sign of $\delta_{i,i+1}$. Lower panel: burst rate evolution when $\beta_i > 0$, corresponding to the red dashed paths in the upper panel. As in Figure 5, we know that $\delta_{i,i}/\gamma_i > \alpha_i > 0$ when it is the slope of the burst rate. The sign of $\delta_{i,i+1}/\gamma_{i+1}$ is not known and the slope sign is determined by the sign of $-\delta_{i,i+1}$.

simulations is well-established around 1–1.2 (see, e.g., Bildsten 1998; Lampe et al. 2016), but the dependence over the other factors should be explored, since information on the values of β and γ_* is scarce and should be measured more accurately. Note that the results from 1D simulations would return the values α, $B = \beta + \alpha$, and $\Gamma = \gamma - 1$ in the case of the dependence over gravity, while in the case of the dependence over mixing, the exponents would be directly α, β, and γ_*. However, one very important point to determine first is the form of the function $\bar{g}_{\rm m}$ (see Sections 2 and 3.1).

This kind of fitting could benefit further from the use of global multidimensional simulations similar to those of Cavecchi et al. (2013, 2015, 2016). Application of the analytical equations determines the most likely ignition colatitude for the burst and indicates whether some part of the star may be covered in partly exhaust fuel. This information could be used in global simulations in order to simulate flame spreading from the most plausible colatitude with a reasonable surface distribution of the fuel. The results could be compared to observed light curves in order to test the agreement of additional details such as, for example, burst oscillations or the exact profile of the light curves of the bursts (see e.g., the discussion in Heger et al. 2007a). Multidimensional simulations would also be key in understanding the differences in local initial conditions, or $\bar{g}$ in our jargon. The advantage introduced by the analytical relations of this paper is to make the comparison between observations and theoretical models faster and possibly even indicate the direction in which to search for refinements in order to match the observational criteria. We have already pointed out one: $\alpha_i + \beta_i/\gamma_{i+1} < 0$.

Future large-area X-ray telescopes, such as the proposed *Enhanced X-ray Timing and Polarimetry* mission (*eXTP*; Zhang et al. 2016) and the NASA Probe-class mission concept *STROBE-X* (Wilson-Hodge et al. 2017), will have improved sensitivity, all-sky monitoring, and spectral-timing capability. Analytical relations of the type given in this paper will be particularly useful to interpret the high-quality sequences of burst and burst oscillation data expected from such missions to understand the details of burning and accretion physics. Combining that with multidimensional simulations will allow a faster and more powerful application of the phenomena associated with thermonuclear explosions to the study of the properties of the underlying NSs, such as, for example the use of type I bursts to tackle the problem of the equation of state of the NS cores (Miller 2013; Watts et al. 2016).

We thank L. Keek for comments on an earlier version of the draft that improved its clarity. Y.C. wishes to thank P. Crumley for asking the right questions. Y.C. is supported by the European Union Horizon 2020 research and innovation programme under the Marie Sklodowska-Curie Global Fellowship grant agreement No. 703916. A.W. acknowledges support from ERC Starting Grant No. 639217 CSINEUTRONSTAR.

Appendix A
What if $\mu_i < 1$?

We stated at the beginning of Section 3 the condition $\mu_i \geqslant 1$, because $\mu_i < 1$ seems highly unlikely. We can explore quickly this alternative here.

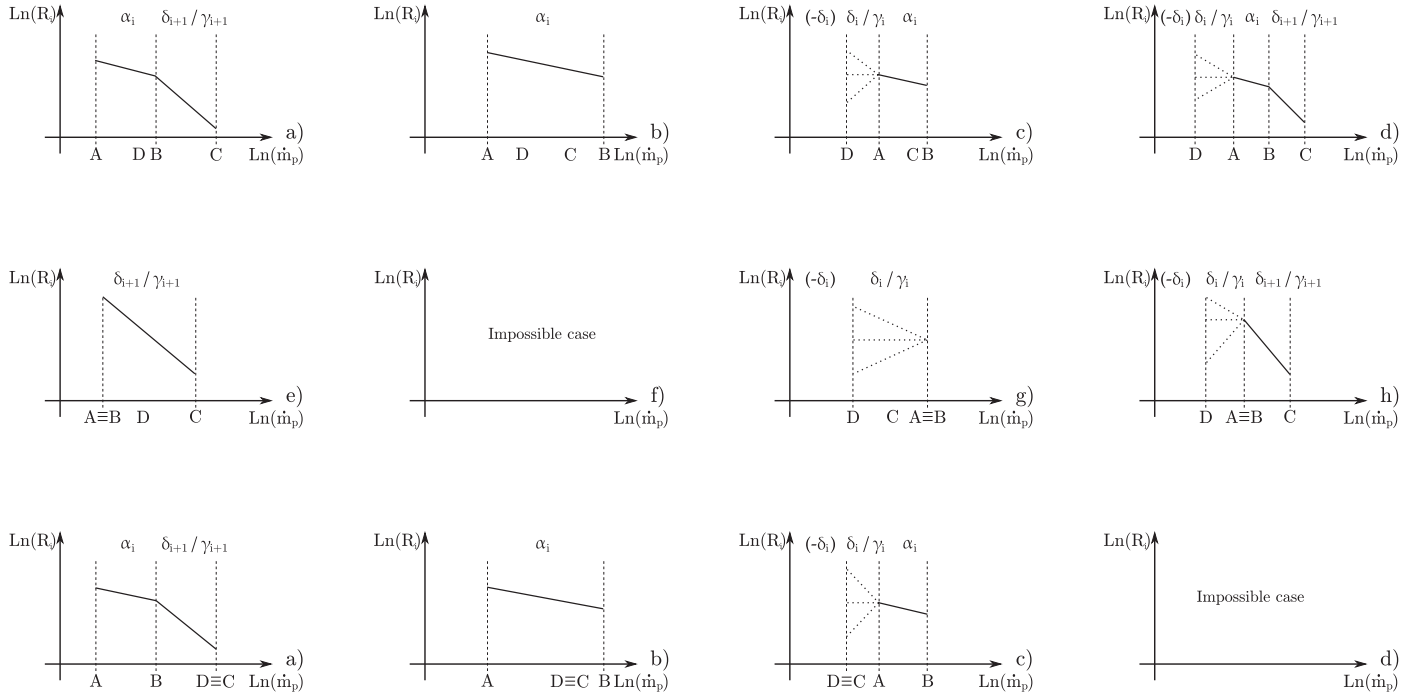

Figure 8. Same as Figure 4, $\beta_i < 0$, but for cases when $\alpha_i < 0$. Top and middle row: these burst rate trends correspond to the blue solid paths in Figure 3. In this case, the sign of $\delta_{i,i+1}/\gamma_{i+1}$ is known when we need it and $\delta_{i,i+1}/\gamma_{i+1} < \alpha_i < 0$. The sign of $\delta_{i,i}/\gamma_i$ is not known when we need it and it depends on the sign of $-\delta_{i,i}$. Bottom row: burst rate corresponding to the blue solid paths of Figure 7, where $\mu_i < 1$.

If $\mu_i < 1$, then the only possibility in order to have an existing window for the bursts is $\Delta\gamma_i > 0$.[14] Then, we can see that Equation (25) constrains $\bar{g}$ to be $\bar{g} \leqslant \epsilon_i^\star$, with $\epsilon_i^\star$ defined as in Equation (28). Since $\epsilon \leqslant \bar{g}$, it follows that $\epsilon \leqslant \epsilon_i^\star$, or, equivalently, we need $\theta_i^\star$, defined as in Equation (31), to exist. In summary,

$$\epsilon \leqslant \bar{g} \leqslant \epsilon_i^\star \;\; if \;\; \mu_i < 1 \;\&\; \Delta\gamma_i > 0 \;\&\; \epsilon \leqslant \epsilon_i^\star. \tag{73}$$

The first conclusion is that when $\mu_i < 1$, ignition at the pole is forbidden. Second, the requirement $\epsilon \leqslant \epsilon_i^\star$ implies that very slow rotators would not show bursts.

We will proceed to study the case $\alpha_i > 0$. The procedure follows very closely the one of Section 3, with the only difference set by the fact that the upper limit is $\epsilon_i^\star$ and not 1. If we study the burst rate evolution for a single source as a function of $\dot{m}_\mathrm{p}$, we obtain Figure 7. The results when $\beta_i < 0$ are identical to the upper panel of Figure 4, apart from the fact that the last case is impossible. When $\beta_i > 0$, the results resemble those of the upper panel of Figure 5, with the loss of the segments corresponding to ignition at the pole and the absence of the last case. Of course, if $\beta_i = 0$, the rate always grows $\propto \dot{m}_\mathrm{p}^{\alpha_i}$.

There is an extra interesting detail. If we think that $\gamma_{i+1} > 0$, the maximum $\dot{m}_\mathrm{p}$ at which bursts will take place is less than the theoretical local one always, even if detectability were not an issue. That is because

$$\dot{m}_{\mathrm{p,\,D\equiv C}} = \dot{m}_{i+1}\,\epsilon_i^{\star\gamma_{i+1}} = \dot{m}_{i+1}\,\mu_i^{\gamma_{i+1}/\Delta\gamma_i} < \dot{m}_{i+1}. \tag{74}$$

In Section 4, we noted how the numerical factor for $\dot{m}_{2,\mathrm{h}}$, the upper bound for the helium ignition in a mixed hydrogen–helium environment, Equation (65), is much smaller than the one for $\dot{m}_{2,\mathrm{l}}$, the lower bound, Equation (60). That led us to explore the possibility $\mu_i < 1$. However, we still deem this possibility less likely than the one treated in the main text.

Appendix B
Extra Cases: $\alpha_i < 0$ and $\alpha_i = 0$

Here we report the extra, less physical cases, $\alpha_i < 0$ and $\alpha_i = 0$, mainly for mathematical completeness.

B.1. Case $\alpha_i < 0$

Both Narayan & Heyl (2003) with linearized calculations and Lampe et al. (2016) with KEPLER simulations found some cases where $\alpha_i < 0$. The window of accretion rates where that happens is relatively small; however, that induces us to discuss this case. The evolution of the bursting rate as a function of $\dot{m}_\mathrm{p}$ for a single source is shown in Figures 8 ($\beta_i < 0$) and 9 ($\beta_i > 0$). In this case, it is known that $\delta_{i,i+1}/\gamma_{i+1} < \alpha_i < 0$ when we need it, while the sign of $\delta_{i,i}/\gamma_i$ is not known for the cases needed: it depends on the sign of $-\delta_{i,i}$ when $\beta_i < 0$ (Figure 8) and on the sign of $\delta_{i,i}$ when $\beta_i > 0$ (Figure 9). When$\beta_i = 0$, the rate always goes $\propto \dot{m}_\mathrm{p}^{\alpha_i}$ decreasing since $\alpha_i < 0$.

[14] Consider Equations (17) and (18): it is needed that $\dot{m}_\mathrm{l}\bar{g}^{\gamma_\mathrm{l}} \leqslant \dot{m}_\mathrm{h}\bar{g}^{\gamma_\mathrm{h}} \Longleftrightarrow \ln(\dot{m}_\mathrm{l}\bar{g}^{\gamma_\mathrm{l}}) \leqslant \ln(\dot{m}_\mathrm{h}\bar{g}^{\gamma_\mathrm{h}}) \Longleftrightarrow 0 \leqslant \ln\mu_i - \Delta\gamma_i \ln\bar{g}$. Since $\ln\mu_i < 0$ and $\ln\bar{g} \leqslant 0$, the inequality is satisfied only if $\Delta\gamma_i > 0$.

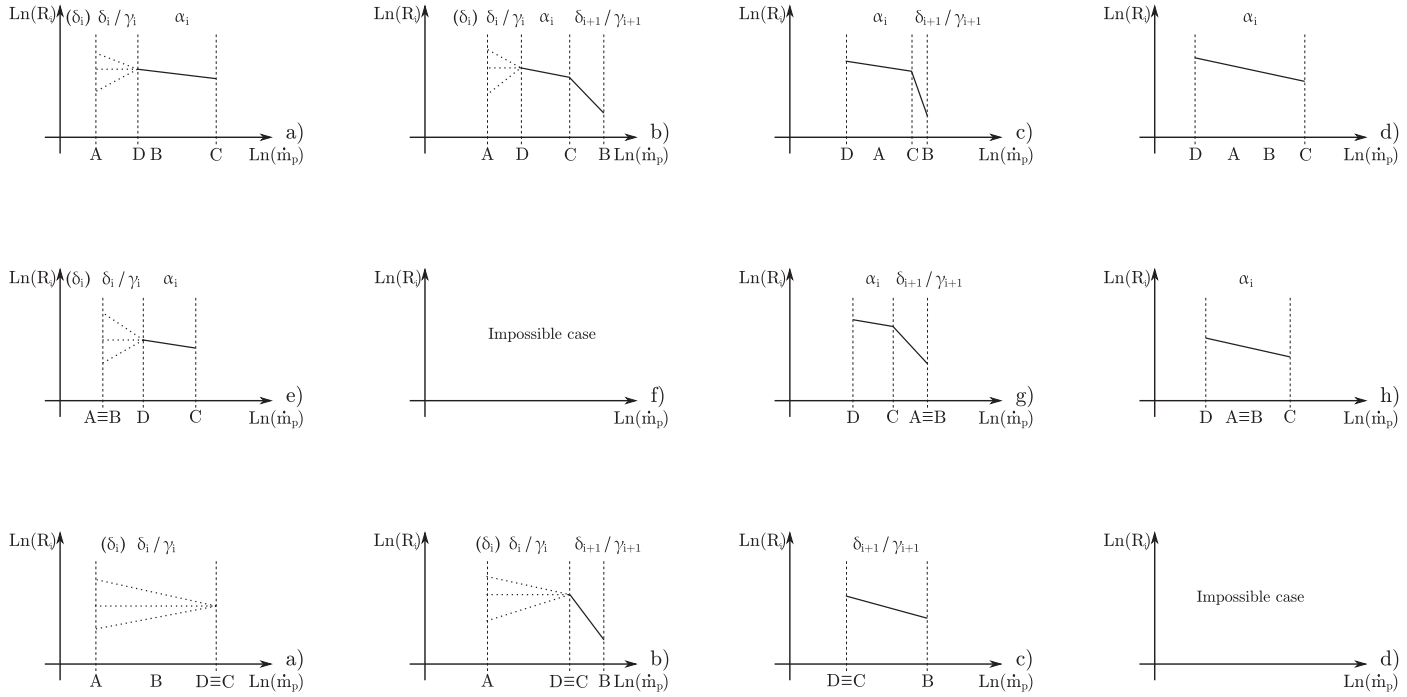

Figure 9. Same as Figure 5, $\beta_i > 0$, but for cases when $\alpha_i < 0$. Top and middle row: these burst rate trends correspond to the red dashed paths of Figure 3. It is known that $\delta_{i,\,i+1}/\gamma_{i+1} < \alpha_i < 0$, although the sign of $\delta_{i,i}/\gamma_i$ is not known when we need it, and it depends on the sign of $\delta_{i,i}$. Bottom row: burst rate corresponding to the red dashed paths of Figure 7, where $\mu_i < 1$.

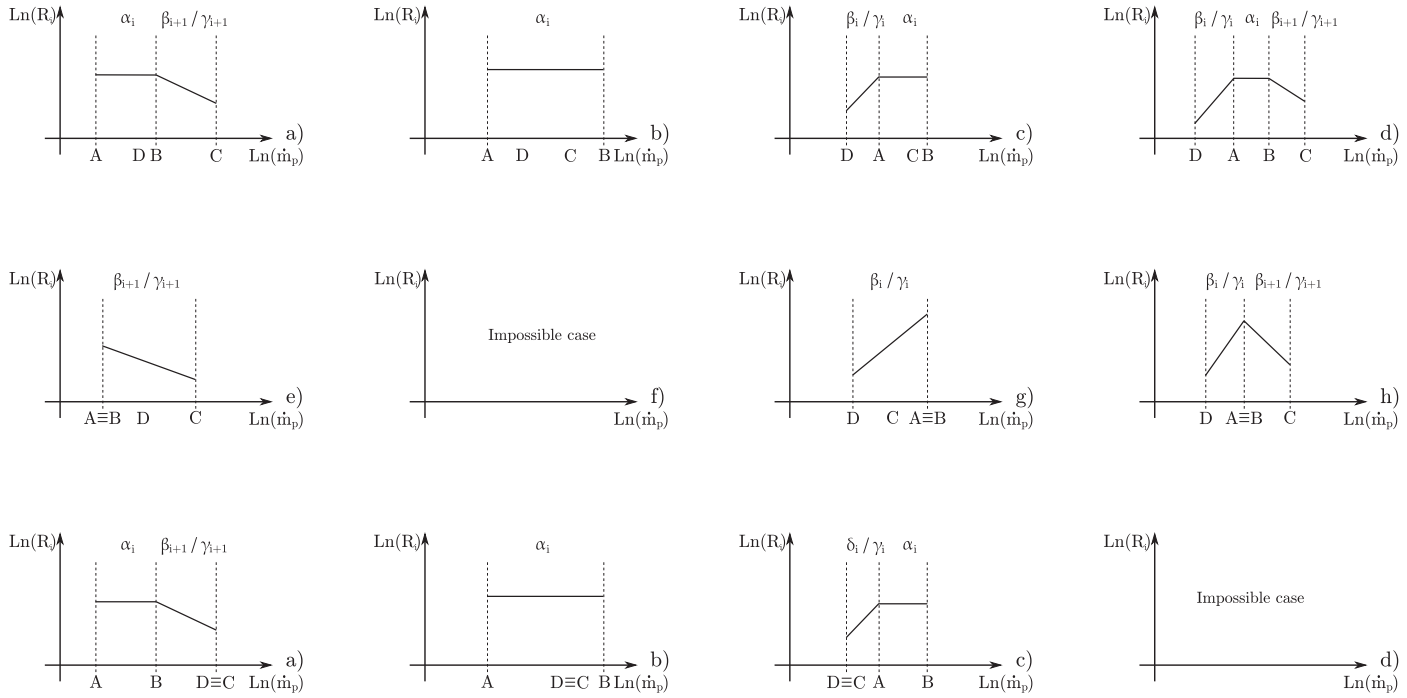

Figure 10. Same as Figure 4, $\beta_i < 0$, but for cases when $\alpha_i = 0$. Top and middle row: these burst rate trends correspond to the blue solid paths in Figure 3. Both the signs of $\delta_{i,i+1}/\gamma_{i+1} = \beta_i/\gamma_{i+1}$ and $\delta_{i,i}/\gamma_i = \beta_i/\gamma_i$ are known. Bottom row: burst rate corresponding to the blue solid paths of Figure 7, where $\mu_i < 1$.

B.2. Case $\alpha_i = 0$

Based on Equation (16), we know that $\mathcal{R} = \bar{\mathcal{R}}_i \bar{g}^{\beta_i}$ for all available ignition colatitudes. This is the most unnatural case, since the burning rate does not depend on $\dot{m}_{\rm p}$, but it changes, of course, depending on the colatitude. The evolution of the bursting rate as a function of $\dot{m}_{\rm p}$ for a single source is shown in Figures 10 ($\beta_i < 0$) and 11 ($\beta_i > 0$). Both the signs of $\delta_{i,i+1}/\gamma_{i+1} = \beta_i/\gamma_{i+1}$ and $\delta_{i,i}/\gamma_i = \beta_i/\gamma_i$ are known when needed. When $\beta_i = 0$, the rate is constant.

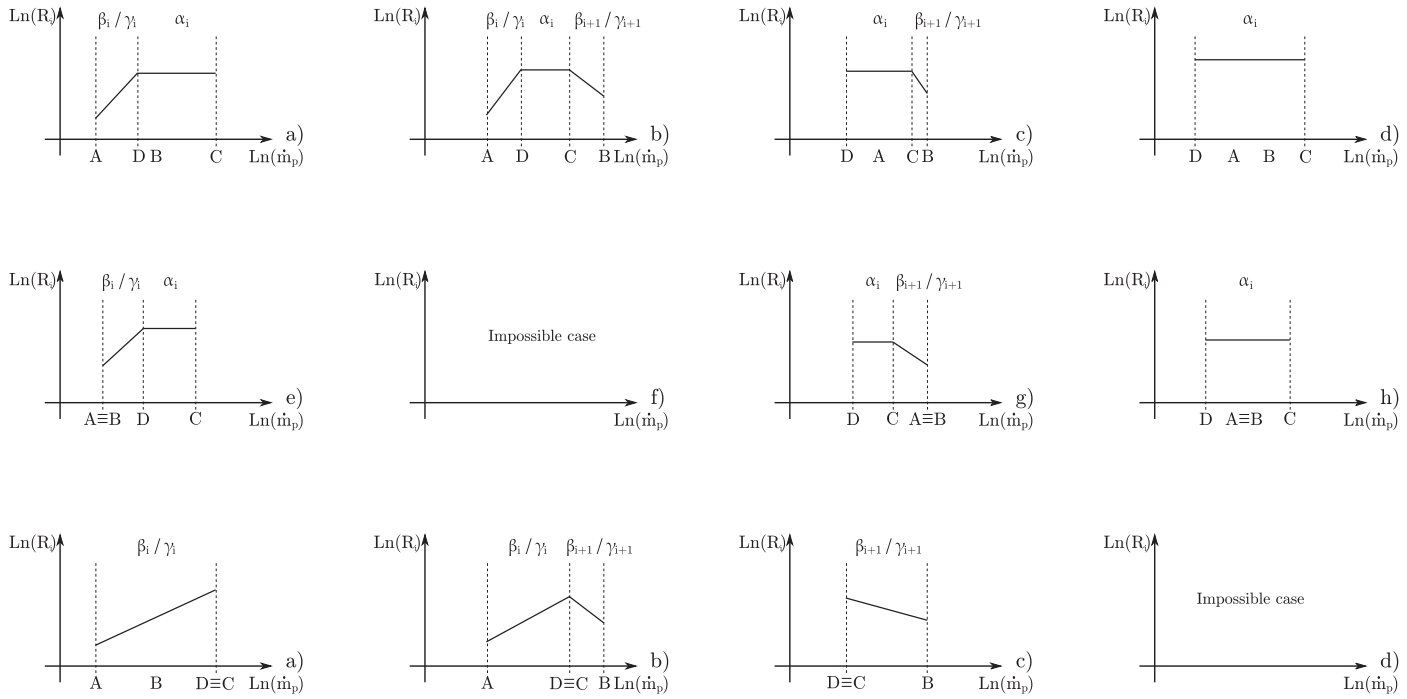

Figure 11. Same as Figure 5, $\beta_i > 0$, but for cases when $\alpha_i = 0$. Top and middle row: these burst rate trends correspond to the red dashed paths of Figure 3. Both the signs of $\delta_{i,i+1}/\gamma_{i+1} = \beta_i/\gamma_{i+1}$ and $\delta_{i,i}/\gamma_i = \beta_i/\gamma_i$ are known. Bottom row: burst rate corresponding to the red dashed paths of Figure 7, where $\mu_i < 1$.

ORCID iDs

Yuri Cavecchi https://orcid.org/0000-0002-6447-3603
Anna L. Watts https://orcid.org/0000-0002-1009-2354

References

AlGendy, M., & Morsink, S. M. 2014, ApJ, 791, 78
Altamirano, D., Watts, A., Kalamkar, M., et al. 2010, ATel, 2932, 1
Bildsten, L. 2000, in AIP Conf. Ser. 522, Cosmic Explosions, ed. S. S. Holt & W. W. Zhang (Melville, NY: AIP), 359
Bildsten, L., & Brown, E. F. 1997, ApJ, 477, 897
Bildsten, L. 1998, in NATO ASIC Proc. 515: The Many Faces of Neutron Stars, ed. R. Buccheri, J. van Paradijs, & A. Alpar (Dordrecht: Kluwer), 419
Brown, E. F., Bildsten, L., & Rutledge, R. E. 1998, ApJL, 504, L95
Brown, E. F., & Cumming, A. 2009, ApJ, 698, 1020
Cavecchi, Y., Levin, Y., Watts, A. L., & Braithwaite, J. 2016, MNRAS, 459, 1259
Cavecchi, Y., Watts, A. L., Braithwaite, J., & Levin, Y. 2013, MNRAS, 434, 3526
Cavecchi, Y., Watts, A. L., Levin, Y., & Braithwaite, J. 2015, MNRAS, 448, 445
Cooper, R. L., & Narayan, R. 2006a, ApJL, 648, L123
Cooper, R. L., & Narayan, R. 2006b, ApJ, 652, 584
Cooper, R. L., & Narayan, R. 2007a, ApJL, 657, L29
Cooper, R. L., & Narayan, R. 2007b, ApJ, 661, 468
Cornelisse, R., in't Zand, J. J. M., Verbunt, F., et al. 2003, A&A, 405, 1033
Cumming, A. 2003, ApJ, 595, 1077
Cumming, A. 2004, NuPhS, 132, 435
Cumming, A., & Bildsten, L. 2000, ApJ, 544, 453
Cyburt, R. H., Amthor, A. M., Ferguson, R., et al. 2010, ApJS, 189, 240
Cyburt, R. H., Amthor, A. M., Heger, A., et al. 2016, ApJ, 830, 55
Davids, B., Cyburt, R. H., José, J., & Mythili, S. 2011, ApJ, 735, 40
Fisker, J. L., Tan, W., Görres, J., Wiescher, M., & Cooper, R. L. 2007, ApJ, 665, 637
Fujimoto, M. Y. 1993, ApJ, 419, 768
Fujimoto, M. Y., Hanawa, T., & Miyaji, S. 1981, ApJ, 247, 267
Galloway, D., in't Zand, J., Chenevez, J., Keek, L., & Brandt, S. 2010, in 38th COSPAR Scientific Assembly, Vol. 38 (Bremen: COSPAR), 2445
Galloway, D. K., Goodwin, A. J., & Keek, L. 2017, PASA, 34, e019
Hanawa, T., & Fujimoto, M. Y. 1984, PASJ, 36, 199
Hartman, J. M., Chakrabarty, D., Galloway, D. K., et al. 2003, BAAS, 35, 865
Heger, A., Cumming, A., Galloway, D. K., & Woosley, S. E. 2007a, ApJL, 671, L141
Heger, A., Cumming, A., & Woosley, S. E. 2007b, ApJ, 665, 1311
Hessels, J. W. T., Ransom, S. M., Stairs, I. H., et al. 2006, Sci, 311, 1901
Inogamov, N. A., & Sunyaev, R. A. 1999, AstL, 25, 269
Inogamov, N. A., & Sunyaev, R. A. 2010, AstL, 36, 848
Kajava, J. J. E., Nättilä, J., Latvala, O.-M., et al. 2014, MNRAS, 445, 4218
Keek, L., Cyburt, R. H., & Heger, A. 2014, ApJ, 787, 101
Keek, L., Langer, N., & in't Zand, J. J. M. 2009, A&A, 502, 871
Lampe, N., Heger, A., & Galloway, D. K. 2016, ApJ, 819, 46
Linares, M., Altamirano, D., Chakrabarty, D., Cumming, A., & Keek, L. 2012, ApJ, 748, 82
Malone, C. M., Nonaka, A., Almgren, A. S., Bell, J. B., & Zingale, M. 2011, ApJ, 728, 118
Miller, M. C. 2013, arXiv:1312.0029
Muno, M. P., Chakrabarty, D., Galloway, D. K., & Psaltis, D. 2002, ApJ, 580, 1048
Narayan, R., & Heyl, J. S. 2003, ApJ, 599, 419
Philippov, A. A., Rafikov, R. R., & Stone, J. M. 2016, ApJ, 817, 62
Piro, A. L., & Bildsten, L. 2007, ApJ, 663, 1252
Schatz, H. 2011, PrPNP, 66, 277
Schatz, H., Aprahamian, A., Barnard, V., et al. 2001, PhRvL, 86, 3471
Schatz, H., Gupta, S., Möller, P., et al. 2014, Natur, 505, 62
Spruit, H. C. 1999, A&A, 349, 189
Spruit, H. C. 2002, A&A, 381, 923
Strohmayer, T., & Bildsten, L. 2006, in New Views of Thermonuclear Bursts, ed. W. H. G. Lewin & M. van der Klis (Cambridge: Cambridge Univ. Press), 113
Tan, W. P., Fisker, J. L., Görres, J., Couder, M., & Wiescher, M. 2007, PhRvL, 98, 242503
van Paradijs, J., Penninx, W., & Lewin, W. H. G. 1988, MNRAS, 233, 437
Watts, A. L. 2012, ARA&A, 50, 609
Watts, A. L., Andersson, N., Chakrabarty, D., et al. 2016, RvMP, 88, 021001
Wijnands, R., Degenaar, N., & Page, D. 2013, MNRAS, 432, 2366
Wilson-Hodge, C. A., Ray, P. S., Gendreau, K., et al. 2017, ResPh, 7, 3704
Woosley, S. E., Heger, A., Cumming, A., et al. 2004, ApJS, 151, 75
Zamfir, M., Cumming, A., & Niquette, C. 2014, MNRAS, 445, 3278
Zhang, S. N., Feroci, M., Santangelo, A., et al. 2016, Proc. SPIE, 9905, 99051Q
Zingale, M., Malone, C. M., Nonaka, A., Almgren, A. S., & Bell, J. B. 2015, ApJ, 807, 60
Zingale, M., Timmes, F. X., Fryxell, B., et al. 2001, ApJS, 133, 195